Article

Effect of Groundwater Extraction and Artificial Recharge on the Geophysical Footprints of Fresh Submarine Groundwater Discharge in the Western Belgian Coastal Area

Marieke Paepen [1],[*] ![ORCID], Wouter Deleersnyder [1,2] ![ORCID], Sybren De Latte [1], Kristine Walraevens [1] ![ORCID] and Thomas Hermans [1] ![ORCID]

[1] Laboratory of Applied Geology and Hydrogeology, Department of Geology, Ghent University, Krijgslaan 281-S8, 9000 Ghent, Belgium; wouter.deleersnyder@kuleuven.be (W.D.); sybrendelatte@hotmail.com (S.D.L.); kristine.walraevens@ugent.be (K.W.); thomas.hermans@ugent.be (T.H.)

[2] Department of Physics, KU Leuven Campus Kortrijk—KULAK, Etienne Sabbelaan 53, 8500 Kortrijk, Belgium

[*] Correspondence: marieke.paepen@ugent.be

Abstract: Human activities, such as managed aquifer recharge (MAR) and groundwater pumping, are influencing the natural groundwater flow in coastal areas. This might induce saltwater intrusion and impact fresh submarine groundwater discharge (FSGD). The use of resistivity methods (electrical resistivity tomography and continuous resistivity profiling) in coastal studies is very effective to investigate the salt–freshwater distribution, but it can be difficult to interpret quantitatively. In this study, the Western Belgian coast is investigated with resistivity methods, and image appraisal tools are systematically used to quantitatively interpret inversion models. Synthetic resistivity models, which reflect the existing situation at the Western Belgian coast, are first created and assessed quantitatively by means of the model resolution matrix, cumulative sensitivity matrix, and depth of investigation index. They reveal that no quantitative interpretation is possible of the FSGD, although lateral qualitative changes can be deduced from the inversion models. The field data show freshwater outflow from the lower beach to below the low water line, and they indicate that MAR has a positive impact on FSGD, while groundwater extraction reduces the outflow of freshwater to the North Sea. A comparison with existing groundwater models indicates their inability to reproduce the actual FSGD footprints.

Keywords: submarine groundwater discharge; continuous resistivity profiling; electrical resistivity tomography; managed aquifer recharge

1. Introduction

The study of submarine groundwater discharge (SGD) to seas and oceans is important in terms of nutrient and pollutant transport to coastal environments and for coastal freshwater management [1]. The outflow can occur from the near-coast zone up to over 80 km offshore for deep confined aquifers [2]. This hidden pathway between land and sea can have any salinity. We can distinguish fresh SGD (FSGD) and saline SGD, as the latter is mainly seawater that recirculates through the seabed.

In this study, we focus on the freshwater component, which is driven by a terrestrial hydraulic gradient, that is, in turn, affected by the hydraulic conductivity of the aquifer [3]. Tides, waves, the buoyancy effect resulting from the density difference between fresh- and saltwater, and dispersion allow the fresh discharge to mix with saline water, resulting in a brackish outflow [4]. The discharge contains both land- and sea-derived nutrients; the latter are more recycled [4]. All these impacting processes lead to temporal and spatial variabilities of SGD.

For decades, the sustainable management of groundwater resources in coastal areas has been the topic of many studies, which searched for ways to optimize pumping rates [5],

check the effect of land use changes [6], and artificially replenish the aquifer [7]. For this, a good understanding of the hydrogeological system is needed. The management of these resources is often based on groundwater models calibrated with land data [8] and, therefore, neglecting SGD.

In coastal areas, the risk of decreasing the groundwater quality by salinization is considerable when pumping rates are too high [9,10]. In order to avoid or mitigate salinization, managed aquifer recharge (MAR) can be used [11,12]. Multiple ways of artificially filling the aquifer with rainwater, surface water, and treated wastewater are possible. Some examples are the use of infiltration ponds, percolation tanks, rainwater harvesting, and underground infiltration boxes [11,13].

These anthropogenic activities will influence the groundwater discharge and alter the salt–freshwater distribution in coastal zones [14]. Pumping reduces the groundwater levels, resulting in a smaller hydraulic gradient between the land and sea, which leads to less FSGD. Groundwater extraction can even lead to saltwater intrusion [9], while MAR will result in the opposite.

In this paper, we assess and compare the footprints of FSGD in front of the municipalities of De Westhoek (De Panne) and Sint-André (Koksijde). Paepen et al. [15] have already established the zones in which FSGD is present west of De Panne (in front of De Westhoek nature reserve) using ERT and CRP. However, the inversion models were not quantitatively checked. The two zones have similar phreatic aquifer characteristics but different management strategies, allowing the impact of anthropogenic activities to be deduced. At Koksijde, groundwater pumping (above 3 million m^3) is combined with MAR, while only limited groundwater extraction occurs at De Panne (pumping rates around 300,000 m^3), where zones that are unaffected by anthropogenic activities also occur. The potable water in the dunes is an important source of drinking water, since salt groundwater is found at a shallow depth in most of the area (i.e., the beach and polder area). Moreover, the water demand is relatively high in this region, especially during the touristic summer season, and, in recent years, more droughts have occurred during the summer, putting the groundwater reserves under pressure.

Although the freshwater outflow is often quite diffuse, zones of (potential) FSGD can be identified using geophysics. Electromagnetics and resistivity methods (electrical resistivity tomography (ERT) on land and marine continuous resistivity profiling (CRP) are particularly suited, given their sensitivity to salinity variations [15–18], but their interpretation can be difficult, especially when the aquifer heterogeneity is not well known or ignored [19].

The non-uniqueness of inversion results allows different resistivity distributions to produce the same calculated response. The inversion process is also driven by subjective modeling parameters, such as the choice of the regularization constraint and the level of noise in the data. The petrophysical relationship is not constant in a heterogenous subsurface, and the resolution of the model decreases with depth [20]. It is, therefore, important to be careful when interpreting the resistivity, which is both spatially and temporally dependent in coastal zones.

Image appraisal tools can be used to address resolution issues, yet they are rarely used in practice, although several approaches are available [21]. They include several aspects, such as recognizing geometries, the identification of noise-associated artefacts, depth of investigation estimation, and the reliability of the inverted parameter (in this case, resistivity) [22]. No commonly accepted methodology exists, but the most-used image appraisal tools to address parameter reliability are the model resolution matrix (*R*), cumulative sensitivity matrix (*S*), and depth of investigation index (*DOI*) [22]. The first two are the most quantitative tools, while the *DOI* is better for qualitative analysis [22].

The reliability of ERT inversion is particularly important in coastal environments, as the smoothing effect of inversion can perturb the interpretation of saline, brackish, and fresh zones. This problem has been considered in a few studies.

Wilson et al. [23] compared 2D ERT data with a prediction of the saline–freshwater interface based on an estimated hydraulic conductivity and gradient using the Glover model, showing that ERT models are more certain in identifying the sharp interface. Comte and Banton [24] cross-validated chloride concentrations from a groundwater model with field apparent resistivities and their inversion results. Nguyen et al. [25] used the data-error-weighted cumulative sensitivity to address the issue of resolution loss with depth in surface-to-borehole ERT in a saltwater intrusion study; they determined a threshold value by synthetic modelling. Beaujean et al. [26] agreed that the matrix of sensitivity is best used for saltwater intrusion cases in terms of both quality and easy implementation and used it to filter out the unreliable part of the tomograms for further interpretation. Hermans et al. [27] compared the ERT image with borehole data to derive a threshold for the sensitivity and showed the influence of the regularization strategy on this threshold. González-Quirós and Comte [19] used a groundwater model to obtain the pore water salinity and calculated the pore water electrical conductivity with a petrophysical model that takes into account the lithological heterogeneity. This information was then used to solved the geoelectrical problem and assess the ability of ERT to identify salinity. Zeynolabedin et al. [28] used a Monte-Carlo uncertainty analysis simulation to obtain the minimum and maximum saltwater intrusion extent from their ERT data.

We focus on the use of geophysics to assess the salt–freshwater distribution. Measurements were taken both on- and offshore to allow a better view of the FSGD zone. The North Sea is a very dynamic environment, characterized by a large tidal range (over 5 m in this area during spring tide) and strong waves, making it challenging for data collection offshore with CRP. The saline SGD component is probably the most dominant due to the tidal activity [29].

Based on the field data of Sint-André and the ground truth data, several synthetic models were constructed, representing the expected distributions of fresh- and salt water offshore and in the intertidal zone. These models allowed a threshold for the quantitative interpretation of ERT and CRP to be defined based on image appraisal tools. This threshold could then be applied to the field data to provide a better understanding of the model resistivities. The improved interpretation results of the inversion models were then compared to the existing groundwater models from De Panne [30] and Koksijde [8] to confirm the pattern from the resistivity measurements.

Our results mainly show that the resistivity of the seawater and the aquifer filled with high-salinity porewater are correctly estimated by the inversion models. The resistivity of the freshwater component is systematically underestimated, making it impossible to draw definite conclusions on the salinity of the FGSD. Nevertheless, our analysis demonstrates that a qualitative interpretation remains possible, as lateral and vertical relative resistivity variations are identified, allowing more saline and more fresh zones to be distinguished. It shows that both land and marine resistivity measurements are useful in real field conditions.

The data, presented here, cover a relatively large part of the Western Belgian coastal zone. Comparing zones without groundwater extraction to locations with groundwater pumping (and MAR) allows us to identify the effect of these anthropogenic activities on FSGD. MAR has a positive effect since the outflow zone extends further offshore compared to when the aquifer is not replenished during groundwater extraction activities.

To our knowledge, this is the first time that such a spatial variation in FSGD can be linked to management strategies. This study, also applies and extends a methodology [22] that allows indirect resistivity data to be reliably and semi-quantitatively interpreted in terms of salinity, which is an important contribution to coastal studies. Finally, we demonstrate that the current local groundwater models, which lack marine data, do not entirely match the FSGD footprint that can be deduced from the resistivity measurements.

2. Study Area

The present 65 km long Belgian coastal zone was formed by an alternation of transgression and regression periods [31,32]. A semi-continuous dune belt, which is up to

2 km wide in the west and lies between the sandy beach and the lower–lying polder area, was established after 700 AD [14]. A natural precipitation surplus allowed the predominantly saline pore water to be flushed out, creating a freshwater lens underneath the dunes [14] (Figure 1). The polder area was reclaimed by man from the North Sea since around 900 AD [33]. The clayey sediments and current artificial drainage of the area have allowed only a little freshening of the polder subsurface. The groundwater flow is mainly from the dunes towards the sea (in the north) and polders (in the south). There is no strong flow along the dune belt.
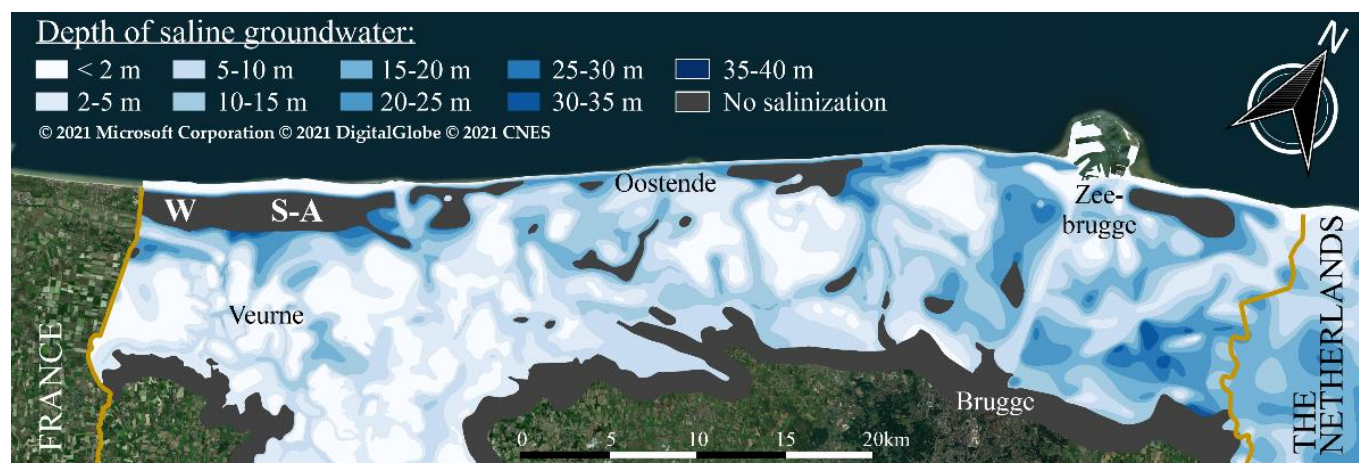

Figure 1. Salinization map of the Belgian coastal phreatic aquifer from De Breuck et al. [34], depicting the depth at which groundwater has a salinity above 1500 mg/L; W and S-A stand for De Westhoek (De Panne) and Sint-André (Koksijde), respectively.

The dunes are widest at Koksijde and De Panne, with an altitude between 6 and 35 mTAW (0 mTAW is the Belgian reference level, which is 2.36 m below mean sea level), and the thickness of the phreatic, sandy aquifer is between 25 and 35 m [35]. This aquifer is bound by the Late Eocene heavy marine clays of the Kortrijk Formation, which are considered impermeable.

The dune belt confines the beach in the north, which is up to 450 m wide during neap tide [35] and has a relatively flat slope. The gently sloping shore and permeable phreatic aquifer, combined with the strong semi-diurnal tides (ranging between approximately 3 and 5.3 m at neap and spring tide, respectively), allows for the occurrence of a saltwater lens under the beach since salt seawater can infiltrate on the back shore during high and spring tide and discharges on the fore shore and/or seabed [36]. Underneath, freshwater coming from the dunes flows towards the North Sea.

The aquifer at Sint-André (Koksijde) consists of (fine) medium sands in which silty or clayey fine sand lenses and organic-rich horizons can occur [35,37] (Figure 2). In the central part of the dunes, the following succession is seen above the Kortrijk clay at well 118DB2 (from bottom to top): a shell layer; layers of loamy fine sand with shells/shell fragments, which are more abundant at the bottom; a second shell layer; fine sand containing a few shells/shell fragments; loamy/clayey fine sand; and medium dune sand with a humus-rich zone [38]. Close to the sea (well 118DB4), the lower aquifer is similar, but the three upper layers are different: medium beach sand containing shells/shell fragments are underlain by a shell layer with finer sand underneath [38]. A shallow clay layer is present in the west of the area [14].
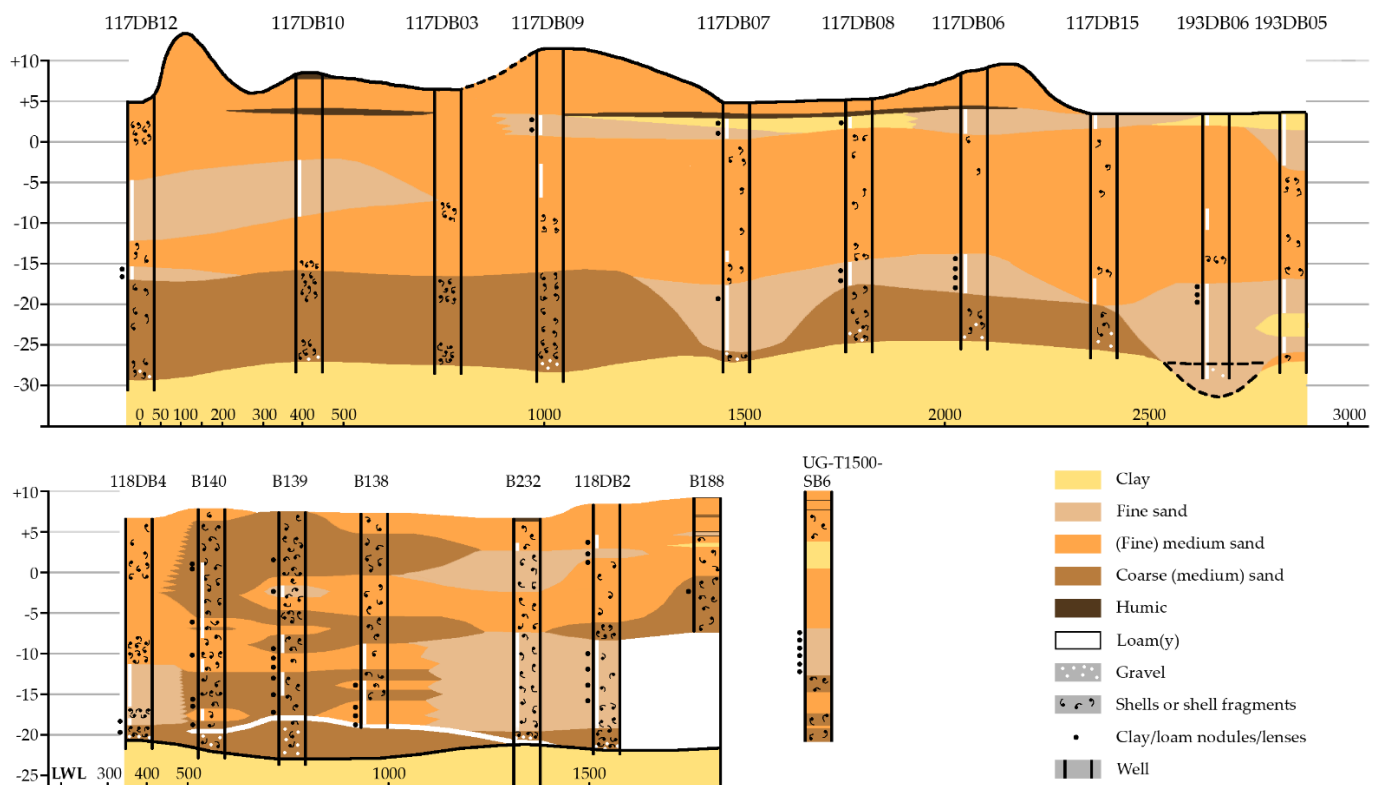
Figure 2. Top: lithological cross section of the dunes of De Westhoek; **bottom**: cross section of the Doornpanne dunes (Koksijde) and borehole UG-T1500-SB6 within Koksijde-Bad. See Figure 3 for the locations of the boreholes. LWL stands for low water line. The top figure was modified from Lebbe [39,40] and the bottom figure is based on borehole descriptions from the Databank Ondergrond Vlaanderen (DOV, Flanders subsurface database).

At 'de Hoge Blekker' (between Koksijde and Oostduinkerke), the public water supply company Aquaduin has an exploitation site where treated wastewater has been artificially infiltrated in two superficial ponds since 2002 [37] (Figure 3). Since November 2014, a shallow 50 m long subsurface infiltration battery was introduced, which was enlarged in 2016 to 300 m [41]. The MAR pond was enlarged in December 2018, and, since March 2019, an old rinse basin has been in use for surface infiltration in the northwest of the site [41]. This all counts for a total of 2.5 million m^3 of wastewater being infiltrated in 2019 and 3.5 million m^3 of drinking water being pumped around well battery 2, at the biggest infiltration pond and subsurface infiltration, in the west [42]. The second infiltration pond (well battery 1, around the old rinse basin) is less important, with 415,000 m^3 of water infiltrated per year, while 900,000 m^3/year is pumped [8]. The artificial recharge increases the groundwater flow towards both the sea and the polder area compared to a situation with only groundwater pumping [43].
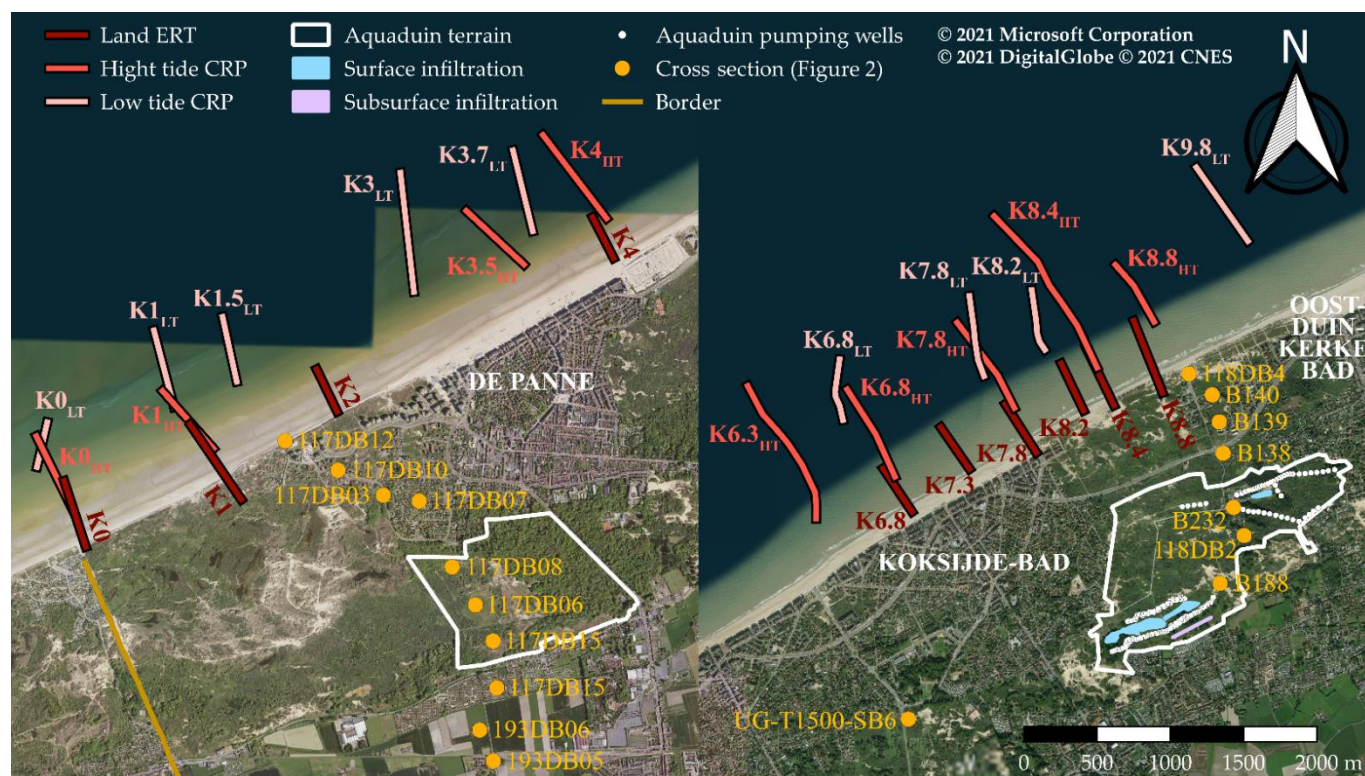
Figure 3. Study areas of De Westhoek (De Panne) (**left**) and Sint-André (Koksijde) (**right**), with the location of the land (burgundy) and marine resistivity profiles (red and pink) and the terrains in which groundwater is extracted from the phreatic aquifer (white lines). The boreholes used in Figure 2 are indicated (orange dots) as well as the position of the surface and subsurface infiltration at Sint-André.

A comparison is made with 'De Westhoek', a European Natura 2000 nature reserve between the municipality of De Panne and the Belgian–French border. Here, the phreatic aquifer is relatively homogeneous close to the Belgian–French border. The upper part contains fine medium sand, and the lower part contains more coarse and medium sands (Figure 2). It becomes more heterogeneous towards De Panne, with the local occurrence of silty fine sand and clay lenses [39,44,45]. The characteristics of the aquifer are relatively comparable to Sint-André (Figure 2). This allows us to assess the impact of other external factors that are affecting the equilibrium between salt and freshwater as well as FSGD, such as groundwater exploitation and artificial recharge in the dunes. The zone near the border is very natural, without any significant anthropogenic influence, whereas in the eastern part of the dunes, groundwater is extracted for drinking water purposes by Aquaduin. The pumping rate was approximately 320,000 m^3 in 2018 and 280,000 m^3 in 2019.

3. Material and Methods

3.1. Electrical Resistivity Tomography

Multiple land ERT surveys were collected at low tides to cover the entire lower beach (Figure 3). Since favorable tide conditions are scarce, the profiles were collected in different seasons and over a period of three years. The measurements were always performed in March–June or September–October since the beach is too crowded during the touristic summer season. In 2018 and 2019, the Terrameter LS (Guideline Geo, Stockholm, Sweden) was used, with 64 electrodes, while the Syscal Pro (Iris Instruments, Orléans, France), with 72 electrodes, was used from 2020 onward. In all cases, the multiple-gradient array was chosen, combined with a spacing of 5 m between the electrodes. This array type allows for a relatively fast data acquisition with multi-channel systems [46], which is critical in the intertidal zone, while maintaining a good signal-to-noise ratio and a good lateral resolution.

Where possible, roll-along was used to create longer profiles. A summary of the collected profiles is shown in Table 1.

Table 1. List of the specifics of the perpendicular resistivity profiles collected at Koksijde and De Westhoek. Each name starts with K (kilometer marker), followed by the approximated distance from the Belgian–French border; HT and LT stand for high and low tide.

Name	Length (m)	Array Type	Electrode Spacing (m)	Date	Figure	Reference
K0	475	Multiple-gradient	5	11 October 2018	11	[15]
K0$_{HT}$	586	Reciprocal Wenner–Schlumberger	15	30 May 2018	11	[15]
K0$_{LT}$	297	Reciprocal Wenner–Schlumberger	10	22 May 2019	11	[15]
K1	625	Multiple-gradient	5	7 March 2018	11	[15]
K1$_{HT}$	517	Reciprocal Wenner–Schlumberger	15	30 May 2018	11	[15]
K1$_{LT}$	537	Reciprocal Wenner–Schlumberger	10	22 May 2019	11	[15]
K1.5$_{LT}$	449	Reciprocal Wenner–Schlumberger	10	22 May 2019	11	[15]
K2	320	Multiple-gradient	5	6 October 2020	12	-
K3$_{LT}$	819	Reciprocal Wenner–Schlumberger	10	22 May 2019	12	-
K3.5$_{HT}$	586	Reciprocal Wenner–Schlumberger	15	30 May 2018	12	-
K3.7$_{LT}$	566	Reciprocal Wenner–Schlumberger	10	22 May 2019	12	-
K4	315	Multiple-gradient	5	12 October 2018	12	-
K4$_{HT}$	717	Reciprocal Wenner–Schlumberger	10	29 May 2019	12	-
K6.3$_{HT}$	1023	Reciprocal Wenner–Schlumberger	10	29 May 2019	9	-
K6.8	360	Multiple-gradient	5	19 March 2021	9	-
K6.8$_{HT}$	699	Reciprocal Wenner–Schlumberger	10	29 May 2019	9	-
K6.8$_{LT}$	419	Reciprocal Wenner–Schlumberger	10	22 May 2019	9	-
K9.3	360	Multiple-gradient	5	16 March 2021	9	-
K9.8	320	Multiple-gradient	5	25 June 2019	9	-
K9.8$_{HT}$	693	Reciprocal Wenner–Schlumberger	10	29 May 2019	9	-
K9.8$_{LT}$	549	Reciprocal Wenner–Schlumberger	10	22 May 2019	9	-
K8.2	360	Multiple-gradient	5	19 March 2021	10	-
K8.2$_{LT}$	410	Reciprocal Wenner–Schlumberger	10	22 May 2019	10	-
K8.4	450	Multiple-gradient	5	22 September 2020	10	-
K8.4$_{HT}$	1254	Reciprocal Wenner–Schlumberger	10	29 May 2019	10	-
K8.8	540	Multiple-gradient	5	21 September 2020	10	-
K8.8$_{HT}$	494	Reciprocal Wenner–Schlumberger	10	29 May 2019	10	-
K9.8$_{LT}$	615	Reciprocal Wenner–Schlumberger	10	22 May 2019	10	-

3.2. Continuous Resistivity Profiling

CRP was chosen to be used at sea, in which a floating cable is towed by a boat, allowing fast and easy data collection (Figure 3). The Syscal Pro Deep Marine (IRIS Instruments, Orléans, France) was used with 195 m (in 2018) and 130 m long (in 2019) cables containing 13 graphite take-outs. The reciprocal Wenner–Schlumberger configuration and a current transmission between 35 and 50 A were used. A Garmin GPSMAP 188 Sounder system (Garmin France, Nanterre, France) provided bathymetry, combined with the boat coordinates, and a conductivity temperature depth (CTD) logger (Van Essen, Delft, The Netherlands) was dragged outside the boat to obtain the seawater conductivity, which is needed to correct for the influence of the seawater layer during the inversion process.

3.3. Inversion and Interpretation

The RES2DINV software was used to invert the land and marine resistivity data [47]. The water layer was included as a soft constraint for the inversion of the CRP profiles, using the bathymetry (multiples and noise were filtered) and seawater resistivity (approximately 0.20 Ωm). The L1 norm was used for both the data misfit and the model constraint to limit the influence of outliers and favor a sharp contrast in resistivity.

The water quality classes of De Breuck and De Moor [48] were used for the interpretation of the resistivity profiles, together with Archie's law,

$$\rho_w = \frac{\rho_b}{F} \tag{1}$$

to convert the bulk resistivity (ρ_b) to the pore water resistivity (ρ_w). A formation factor (F) was estimated for both zones, which was 3.2 for De Westhoek [39] and 4 at Sint-André [8]. We distinguish between fresh- (higher than 20 or 25 Ωm respectively), brackish, and salt water (below 2.5 or 3.125 Ωm respectively).

3.4. Image Appraisal Tools

In this study, we aimed to assess the reliability of inversion based on the methodology proposed by Caterina et al. [22], which was adapted for the specific evaluation of salinity in coastal settings. It consists of six steps (Figure 4):

(1) Field data is acquired for which a real inverted model is obtained.
(2) A real synthetic model is defined, which resembles the real inverted model and includes known ground truth data.
(3) After forward modelling of this model, the simulated data is inverted to obtain a synthetic inverted model. The same inversion parameters (electrode array, inversion parameters, etc.) are used as for the field data, and the *DOI*, *R*, and *S* are calculated (see Sections 3.4.1–3.4.3).
(4) The real synthetic model and the synthetic inverted model are compared, allowing the evaluation of the absolute error on the salinity fraction (Δf_s, between 0 and 1), which is used to define the bulk resistivity (ρ_b):

$$f_s = \frac{\rho_b - \rho_{b,f}}{\rho_{b,s} - \rho_{b,f}} \tag{2}$$

$$\Delta f_s = f_{s,\text{synthetic model}} - f_{s,\text{inversion model}} \tag{3}$$

for which we used 0.1969 Ωm as the bulk saltwater resistivity ($\rho_{b,s}$) and 50 Ωm to represent the bulk freshwater resistivity ($\rho_{b,f}$).

(5) The error is evaluated against the *DOI*, *R*, and *S* to define a threshold.
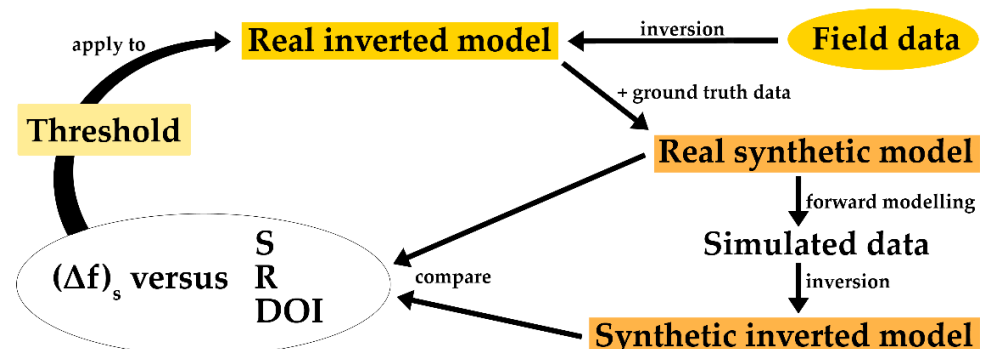(9) The thresholds can be applied to the real inverted model.

Figure 4. Flowchart of the image appraisal methodology.

Next to the quantitative analysis of image appraisal, we complement the approach of Caterina et al. [14] with an analysis of the ability of ERT and CRP to qualitatively detect lateral variations in resistivity. Paepen et al. [15] showed that, although the inversion might not be sufficiently accurate to interpret the absolute resistivity values in the tomogram, for FSGD studies, relative lateral variations are likely good indicators of the presence of fresher water in the aquifer.

3.4.1. Depth of Investigation (*DOI*)

The *DOI* concept introduced by Oldenburg and Li [49] is used to define a depth below which the data is no longer sensitive to the earth structures. It is a qualitative tool and is not quantitative [22]. Two additional inversions (*m*1 and *m*2) are needed to see how much the data depend on the property of the subsurface by using 0.1 and 10 times the reference resistivity of the original inversion (m_{ref1} and m_{ref2}). We followed Caterina at al. [22] by using a damping factor of 0.05 for these reference models. Differences between the models quantify the *DOI*:

$$DOI = \frac{|\log(m1) - \log(m2)|}{\left|\log\left(m_{ref1}\right) - \log\left(m_{ref2}\right)\right|} \tag{4}$$

A large variation (high *DOI*) will indicate that the data is less sensitive to the Earth's resistivity. The visual comparison between the models also helps when assessing structures that are systematically present in the inversions and, hence, qualitatively estimate the robustness of the method to detect relative variations in resistivity [15].

3.4.2. Model Resolution

Numerous factors influence the model resolution, such as the resistivity distribution, electrode geometry, and noise [21]. The resolution in Res2dinv is calculated at the last iteration of the inversion using the following formula:

$$R = \left[J^T J + \lambda \cdot \left(\alpha_x C_x^T C_x + \alpha_z C_z^T C_z\right)\right]^{-1} \cdot J^T J \tag{5}$$

based on the Jacobian sensitivity matrix (J), the damping factor (λ), and the horizontal and vertical roughness filters (C_x and C_z respectively) with their corresponding weights (α_x and α_z). T is the transpose operator [47].

3.4.3. Cumulative Sensitivity

The cumulative sensitivity matrix (S) is a computationally inexpensive alternative for the model resolution matrix:

$$S = \left(J^T W_d^T W_d J\right)_{jj} \tag{6}$$

This method [21,50] is widely used, since the Jacobian matrix (J) is directly available after the inversion. W_d is the data weighting matrix. Higher sensitivities are evidence for better-constrained inverted values.

3.5. Existing Groundwater Models of the Area

The resistivity data was compared to existing models of the De Panne [30] and Koksijde [8] areas. Both models are density-dependent models with model cells of 75 by 75 by 2.5 m that were calibrated using hydraulic heads in the vicinity of the extraction facilities. Natural boundary conditions were chosen in the polders and at sea, while the models were extended sufficiently laterally to avoid an impact on the hydraulic heads in the extraction zone and to impose no flow conditions. The boundary conditions were static, meaning that no tidal activity was considered on the seaside. The aquifer recharge was estimated at 252 mm/year, and the simulated extraction rates were provided by Aquaduin.

4. Results

4.1. Synthetic Models

Based on the situation already observed at De Westhoek [15], we expected two situations at Sint-André (or intermediate conditions): discharge of brackish to fresh water on the lower beach or further offshore. In both cases, a saltwater lens was expected to lie above the freshwater between the discharge zone and the dunes. Based on this prior knowledge, we designed five synthetic cases that we analyzed with the methodology described in Section 3.4.

The resistivities of the synthetic models were based on earlier research. The Kortrijk Formation clay (2.5 Ωm) was deduced from resistivity well logging of borehole kb11d35e-B146 (from DOV, Flanders subsurface database). The CTD diver, used for the CRP surveys, allowed the estimation of the seawater resistivity (0.1969 Ωm). The aquifer resistivities when filled with salt (0.95 Ωm) or freshwater (50 Ωm) were derived from well loggings on the beach of Westhoek by Lebbe [51] and were corrected for the formation factor of Sint-André, and the mixing zone between the two was estimated at 5 Ωm.

A first synthetic model (S1) of the intertidal zone was created: a sandy aquifer bound by clay, with freshwater discharge on the lower beach (Figure 5). A saltwater lens is present, underlain by the freshwater which comes from the dunes. After inversion the overall salt and freshwater distribution is similar to the synthetic case. Yet, the boundary between the freshwater lens and clay layer is not a sharp transition and is located deeper than its location in the synthetic model. The mixing zone between the salt and freshwater is not visible in the inversion model. The resistivity of the freshwater is lower in most areas, especially where the thickness of the saltwater lens is largest: 92 percent of the freshwater lens has a resistivity below 50 Ωm after inversion (see histogram). This is due to the lower sensitivity and resolution, caused by the loss of signal in the highly conductive layer and due to the smoothing by the regularization process. Finally, the clay resistivity is different from the synthetic model, it is higher after inversion as a result of the loss of resolution and the presence of a more resistive freshwater layer on top of it. The absolute error of the salinity fraction is largest in the freshwater zone where the overlying saltwater lens is thickest and at the interfaces of fresh-/saltwater and clay/freshwater.

The normalized sensitivity and resolution have similar patterns, they are decreasing with depth, as expected. The *DOI* is less easily interpreted, only the saltwater layer has a consistently low *DOI*, while the other zones are more heterogeneous. The plots in Figure 5 show the relationship between the salinity fraction error and the normalized sensitivity, resolution, and *DOI*. Similar to Caterina et al. [22], a moving average was taken for the normalized sensitivity, resolution, and *DOI* to visualize the main trends. A window of 100 points was chosen, but a different range for averaging will affect the threshold. For the *DOI*, the error is consistently above 0.1, even for low *DOI* values, which is too large for a good quantitative assessment.

The threshold, from which the average error of the salinity fraction increases rapidly, can be chosen at an error of 0.05 for both the normalized sensitivity and resolution (Figure 5, blue lines). All inversion model cells with a normalized sensitivity above 0.056 or a resolution higher than 0.073 provide a good quantitative (i.e., with an error lower than 0.05) measure for the resistivity. This is mainly the upper part of the inversion model, the saltwater lens and a small portion of the outflow zone on the lower beach. When selecting a higher threshold, e.g., 0.1, the zone for quantitative appraisal only slightly increases in size, changing nothing in the interpretation of the land inversion model. This is consistent with the choice of the threshold corresponding to a sharp increase in the error.
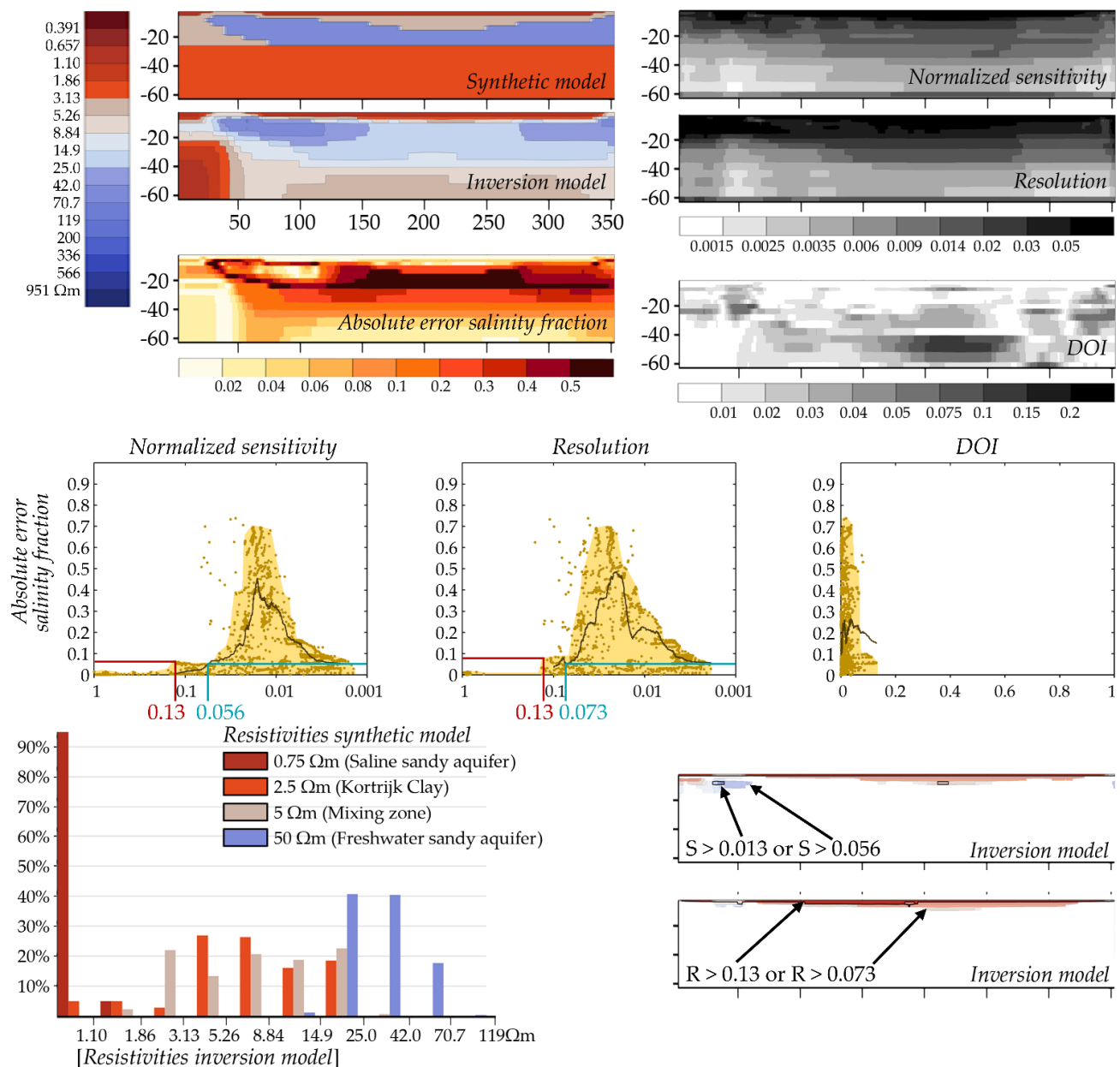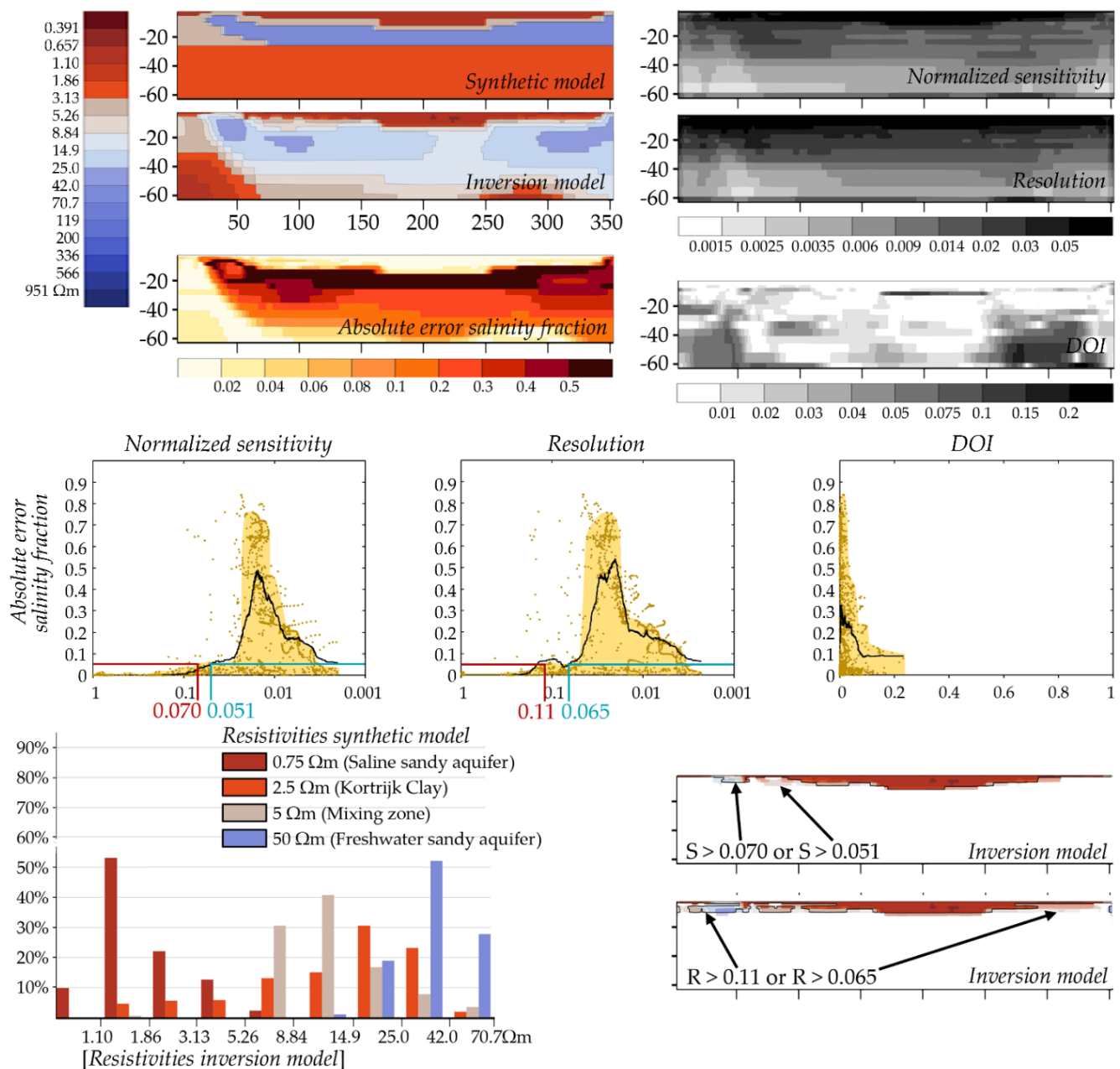
Figure 5. Synthetic model S1, land aquifer with freshwater outflow on the lower beach. The blue thresholds on the graphs show the boundary for quantitative interpretation based on the methodology of Caterina et al. [22] (the average shown by the black line), while the red lines are based on the maximal salinity fraction error (indicated by the extent of the yellow shape).

As an alternative to a threshold based on the average error, we proposed to also check the maximal values, neglecting individual outliers, to define the threshold (Figure 5, red lines). This allows a more conservative estimation to be made of the zone that can be quantitatively interpreted, compared to the average, which is a more optimistic approach. For model S1, the normalized sensitivity and resolution thresholds becomes 0.13, corresponding to the first point for which the 0.05 error is exceeded. The overall area for quantitative appraisal slightly decreases in size with this threshold, containing the highest meter(s) of the beach.

In a second synthetic model, we increase the thickness of the saltwater lens (S2, Figure 6). The freshwater tongue inverted resistivity decreases compared to S1, especially below the thickest part of the saltwater lens. The boundary between the freshwater and clay is more difficult to identify. It appears deeper compared to model S1 and seems to

be dipping towards the dunes. Moreover, only 10% of the original saltwater lens has a resistivity below 1.10 Ωm after inversion (see histogram), while this is 95% for S1.
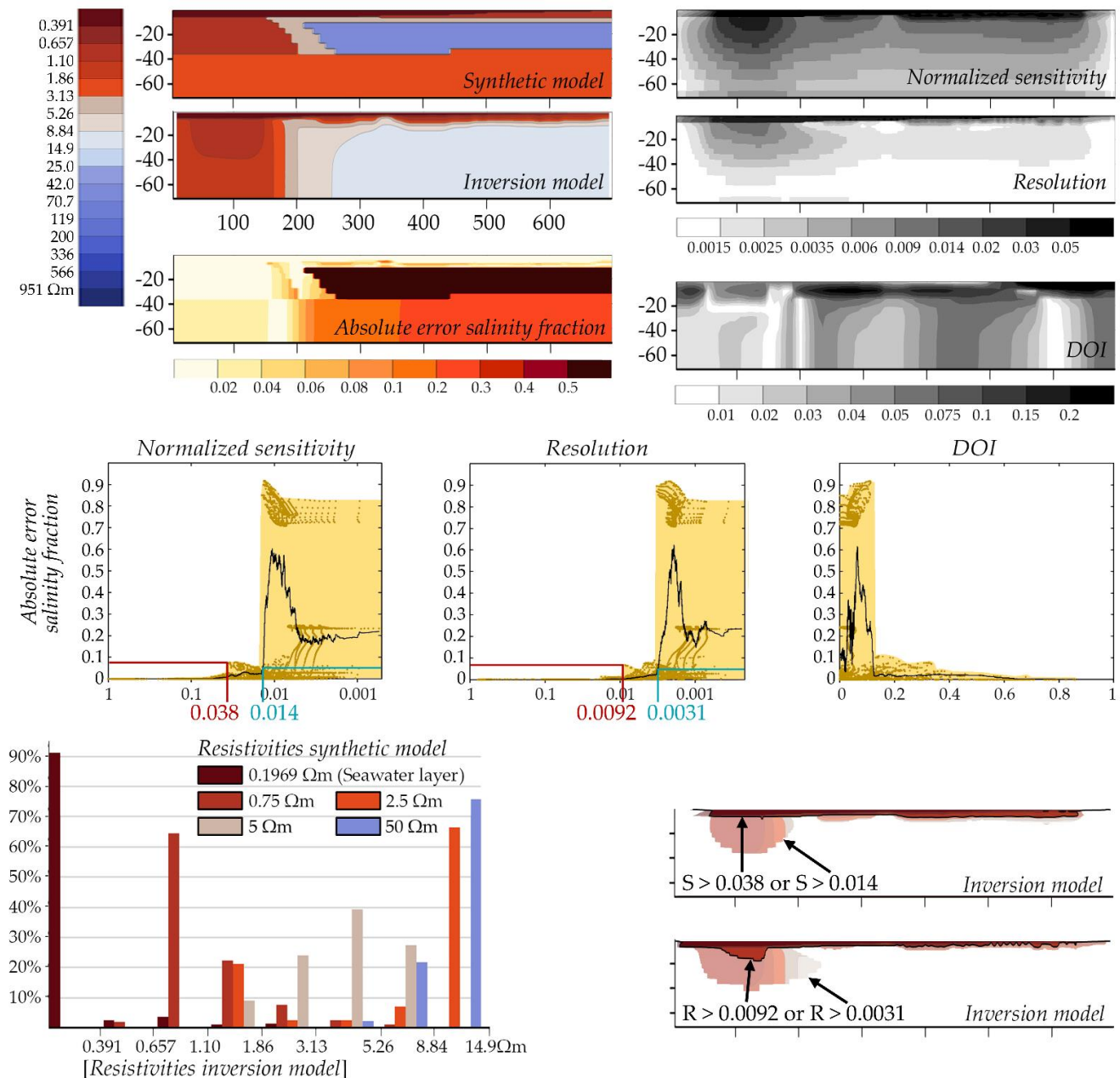

Figure 6. Synthetic model S2, the saltwater lens thickness is increased compared to S1. The blue thresholds on the graphs show the boundary for quantitative interpretation based on the methodology of Caterina et al. [22] (the average shown by the black line), while the red lines are based on the maximal salinity fraction error (indicated by the extent of the yellow shape).

When picking a threshold of 0.05 for the salinity fraction error, the corresponding normalized sensitivity (0.051) and resolution (0.065) are similar to S1. The top of the saltwater lens and the discharging zone on the lower beach can be quantitatively interpreted. Note, however, that, given the largest thickness of the saltwater lens, the absolute depth for which interpretation can be quantitative is slightly larger compared to S1. For the *DOI*, the average salinity error threshold of 0.05 is exceeded for all *DOI* values (for both the average and maximal values) and, thus, for all cells of the inversion model and is, therefore, not suited for this purpose. When using the maximal salinity errors, the normalized sensitivity

threshold is increased to 0.070, and it is 0.11 for the resolution. This does not change the interpretation of the model resistivities much.

Synthetic models S3 and S4 (Figures 7 and 8) correspond to a marine aquifer with FSGD. They differ by the thickness of the seawater layer. After inversion, the clay layer is no longer visible. The freshwater resistivity, after inversion, decreases even more compared to models S1 and S2. The resistivity of the entire freshwater tongue is underestimated in the inversion model. The whole freshwater lens also displays the largest error on the salinity fraction. Since much of the electrical signal is lost in the highly conductive seawater layer, the resistivity of the freshwater lens is not properly recovered.

Figure 7. Synthetic model S3, marine aquifer with freshwater outflow. The blue thresholds on the graphs show the boundary for quantitative interpretation based on the methodology of Caterina et al. [22] (the average shown by the black line), while the red lines are based on the maximal salinity fraction error (indicated by the extent of the yellow shape).
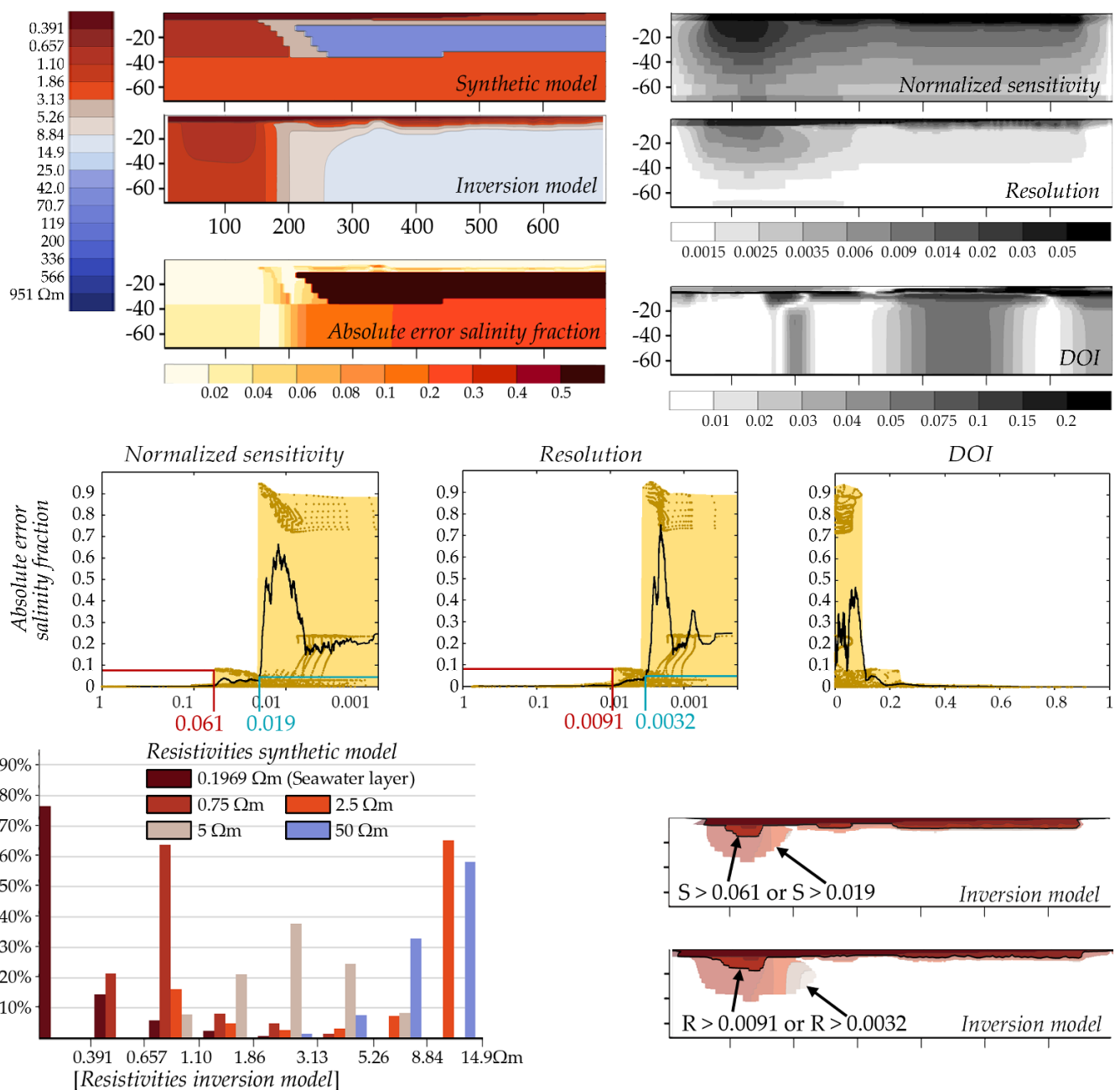
Figure 8. Synthetic model S4, the bathymetry is approximately 1 m deeper compared to S3. The blue thresholds on the graphs show the boundary for quantitative interpretation based on the methodology of Caterina et al. [22] (the average shown by the black line), while the red lines are based on the maximal salinity fraction error (indicated by the extent of the yellow shape).

The normalized sensitivity and resolution decrease quickly below the seawater layer. For model S3, the corresponding normalized sensitivity and resolution to an average salinity fraction error threshold of 0.05 are 0.014 and 0.0031, respectively, which is similar to model S4, in which they correspond to 0.019 and 0.0032. These thresholds allow a quantitative interpretation for the seawater layer and the sandy aquifer more offshore to the freshwater discharge, i.e., when it is filled with salt porewater. For the *DOI*, several low values correspond to a very high salinity fraction error, while high values are observed in the upper part of the model where the error is low. We expect this is a result of the sensitivity of the inversion results to the presence of the seawater layer [9]. This result is in

opposition to the sensitivity and resolution and confirms that the *DOI* is not suited for a quantitative appraisal of the inversion results.

The interpretation is much different when assessing the maximal salinity fraction errors. Then, the threshold of 0.05 is already exceeded at a normalized sensitivity of 0.038 and 0.061 and a resolution of 0.0092 and 0.0091 for models S3 and S4, respectively. This greatly decreases the zone in which the resistivity can be interpreted quantitatively. It now contains a smaller zone of the saline aquifer and almost the same part of the seawater layer.

Based on those results, the only part of the model that can be interpreted quantitatively corresponds to the seawater and a part of the saline aquifer. To be sure that the marine data is sensitive to the presence of FSGD, a last synthetic model (S5) is introduced in which the aquifer only contains salt porewater (Figure 9). After inversion, the entire seabed has a resistivity below 1.4 Ωm. Due to the absence of FSGD, there is no salinity fraction error above 0.05, meaning that the whole section can be interpreted quantitatively.
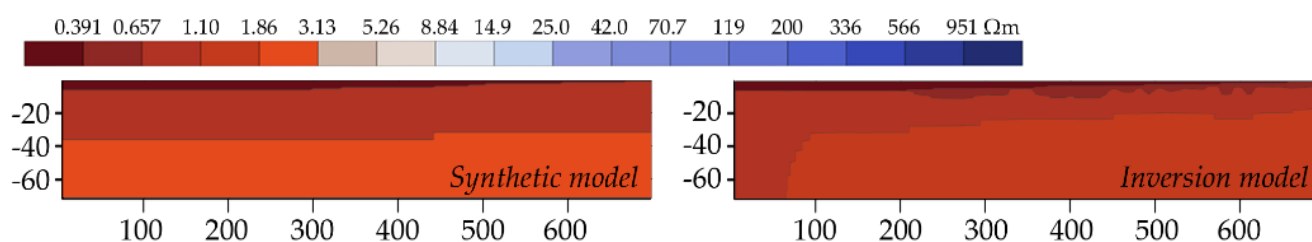
Figure 9. Synthetic model S5, marine aquifer without freshwater outflow and its inversion model.

Considering the difference in the inverted results between Figures 7 and 9, it is clear that the relative lateral changes in resistivity are qualitatively resolved by ERT as well as the vertical transition from salt- to freshwater, although the salinity fraction cannot be quantitatively interpreted. If the field data resembles S5 after inversion, it is likely that there is no FSGD present. If not, a quantitative interpretation is possible based on the threshold deduced above, while a qualitative interpretation is possible of the lateral and, to a lesser extent, vertical resistivity contrasts.

In summary, a low error on the estimation of the salinity fraction (below 0.05) allowing a quantitative interpretation from the geoelectrical methods is limited to the shallow subsurface on land (up to 5 m deep). Offshore, it is restricted to the seawater layer and the phreatic aquifer filled with salt porewater. A quantitative interpretation of the freshwater tongue in terms of salinity is, therefore, only possible in a very small portion of the land models (S1 and S2, Figures 6 and 7). The inverted freshwater resistivity in the other zones is underestimated. On land, the salinity error is largest at the interfaces between salt and freshwater and freshwater and the underlying clay, making it difficult to localize these transitions precisely. A thicker saltwater lens leads to an increase of the error on the salinization fraction as a result of smoothing during inversion. At sea, the freshwater tongue has the highest salinity fraction error for the entire model. A small error on the bathymetry (in the order of 1 m) has a limited influence on the interpretation of marine CRP (Figures 7 and 8).

Although the quantitative interpretation of the resistivity data is limited, the synthetic models show that the variations of resistivity can be consistently interpreted qualitatively. When accounting for all inversion limitations observed with the synthetic cases, it is possible to detect the occurrence of freshwater below a saline lens. The lateral transition from saline to freshwater can be seen both on land and offshore, without being able to estimate the salinity with confidence everywhere.

4.2. Field Data

We now apply the selected thresholds to the field data (Figures 10 and 11). As the *DOI* has been shown to be inadequate to provide a quantitative assessment, and the resolution and sensitivity provide similar results, we use the normalized sensitivity for

image appraisal. For land profiles, we select the threshold of 0.13 for the normalized sensitivity, derived from model S1 and corresponding to the maximum error, as it is more conservative than using the average error or the threshold derived for model S2. Only the resistivities above the black lines can be quantitatively interpreted. This includes the saltwater lens and the top part of the dune sediments. For the offshore profiles, a normalized sensitivity of 0.038, derived from model S3, is used. The area above the black line never includes the brackish lens, which extends offshore. It only comprises the seawater layer and a part of the saline aquifer. This means that no quantitative measure for the discharge's salinity can be derived from the inversion models.
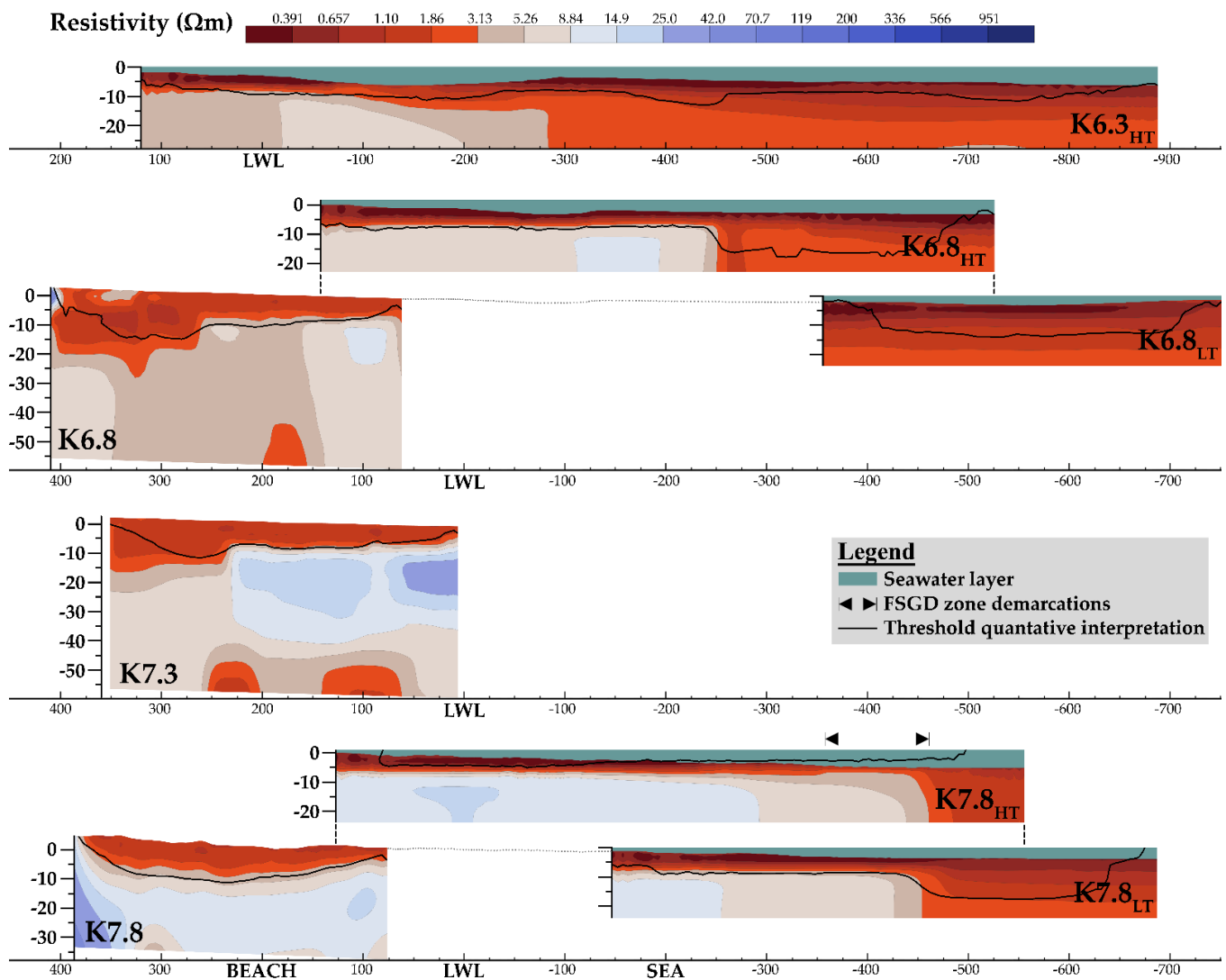
Figure 10. Land and marine ERT inversion models in front of Koksijde-Bad. LWL, HT, and LT stand for low water line, high tide, and low tide, respectively; the black lines are the thresholds above which a quantitative interpretation is possible; all profiles have the same scale length.
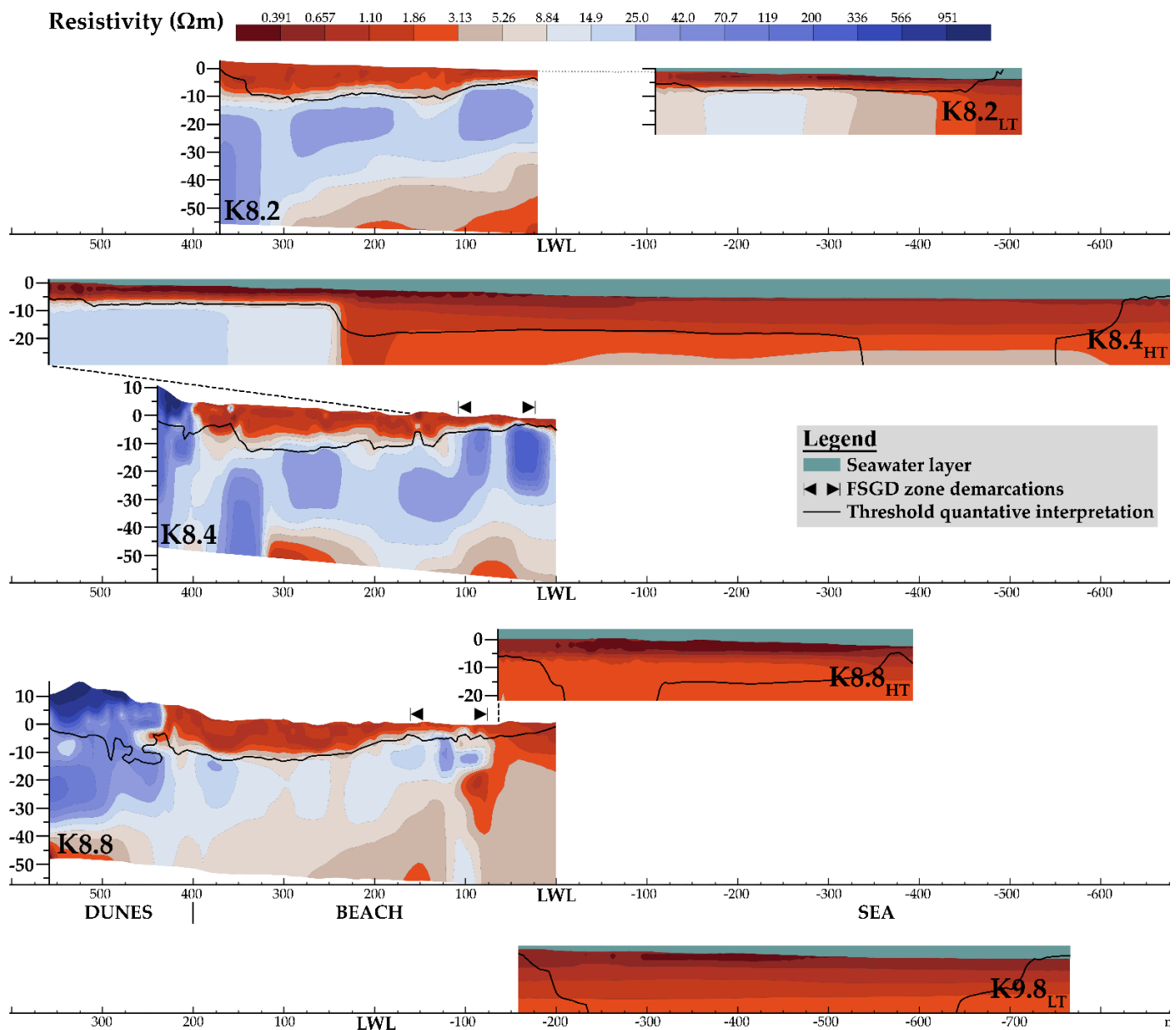
Figure 11. Land and marine ERT inversion models in front of the dunes between Koksijde-Bad and Oostduinkerke-Bad. LWL, HT, and LT stand for low water line, high tide, and low tide, respectively; the black lines are the thresholds above which a quantitative interpretation is possible; all profiles have the same scale length.

In front of the municipality of Koksijde-Bad (in the west), there is no freshwater outflow on the beach (Figure 10, K6.8 and K7.3). The aquifer does contain more brackish to fresh pore water below a saltwater lens, which becomes thinner towards the North Sea. The freshwater lens cannot be quantitatively interpreted, and the thick saltwater lens (up to 20 m) above leads to a lower inverted resistivity as a result of smoothing. Further offshore, the subterranean estuary is filled with brackish pore water (Figure 10, K6.8$_{HT}$), hinting at an outflow of groundwater (due to the buoyancy effect) up to approximately 250 m away from the low water line.

A similar pattern is seen in front of Aquaduin's largest infiltration pond (Figure 10, K7.8, K7.8$_{HT}$, and K7.8$_{LT}$). Yet, the saltwater lens is much thinner (up to 10 m), allowing the inversion to retrieve a higher and more homogenous resistivity underneath, although it is still below the threshold for quantitative interpretation. No freshwater discharge is seen on the beach, but outflow is visible with CRP (Figure 10, K7.8$_{HT}$), for which the top,

more saline part of the subterranean estuary is thinner between 350 and 450 m offshore, indicating an upward flow of the brackish pore water. Essentially, only the resistivity of the seawater layer is realistic. It is possible that the outflow is fresher than deduced from the inversion model, as resistivity values tend to be underestimated by the inversion, as shown in model S3 and S4.

Further east, the saltwater lens is still not cut off by FSGD on the beach, and the brackish pore water is extending up to 425 m below the low water line (Figure 11, K8.2 and K8.2$_{LT}$). The saltwater lens on the beach extends up to 10 m deep, similar to K7.8, but the resistivity of the freshwater lens is larger.

At 8.4 km from the border, there is an upwelling of brackish/freshwater on the lower beach between approximately 25 and 100 m above the low water line, overlain by a thin saltwater layer (Figure 11, K8.4). Up to around 195 m offshore, the subterranean estuary contains brackish porewater (Figure 11, K8.4$_{HT}$), which is not as far offshore as in K7.8 and K8.2. This more resistive part of the model is no quantitative measure for the resistivity of the aquifer, as it remains below the threshold of sensitivity. At K8.8 (Figure 11, K8.8$_{HT}$), brackish/freshwater is mainly found in the intertidal zone, discharging between approximately 50 and 150 m above the low water line. Below the low water line, no brackish water is seen. The seaside of the land model does show a higher resistivity than salt water. This is likely due to either the low data coverage in this part of the model and/or the clay layer's influence. At K9.8 (Figure 11, K9.8$_{HT}$), no outflow is seen offshore.

The Belgian–French border (K0) gives an idea on the natural FSGD footprint in the western coast (Figure 12). Paepen et al. [15] showed that there is no freshwater discharge on the beach. The outflow only occurs below the sea level, with discharge likely occurring from approximately 250 m offshore from the low water line and further offshore. However, 1 km to the east ([15], K1), outflow is seen both on the lower beach (25–125 m above the low water line) and offshore (between 200 and 300 m below the low water line). Brackish pore water is seen until 550 m from the low water line. The pore water quality of the brackish/freshwater tongue below the low water line is fresher at K0 compared to K1 after inversion, which can be caused by the discharge of a portion of the fresh groundwater on the beach at the latter location, in which case the water is actually fresher at K0. Another explanation is the thinner portion of the seabed filled with saltwater on top, in which case the apparent fresher water is an artifact of inversion, since this part of the model cannot be interpreted quantitatively.

Further to the east, discharge is still seen on the lower beach (Figure 13, K2 and K4). At the same time, the discharge does not reach (very far) offshore from K3 to K4 (Figure 13). This is possibly due to the extraction (pumping mainly occurs in the eastern part of the Aquaduin site, Figure 3), which moves the water divide to the north, decreasing the recharge zone of the freshwater tongue and/or due the influence of the municipality of De Panne (where there is a higher number of impermeable surfaces, such as roads, walkways, and roofs).
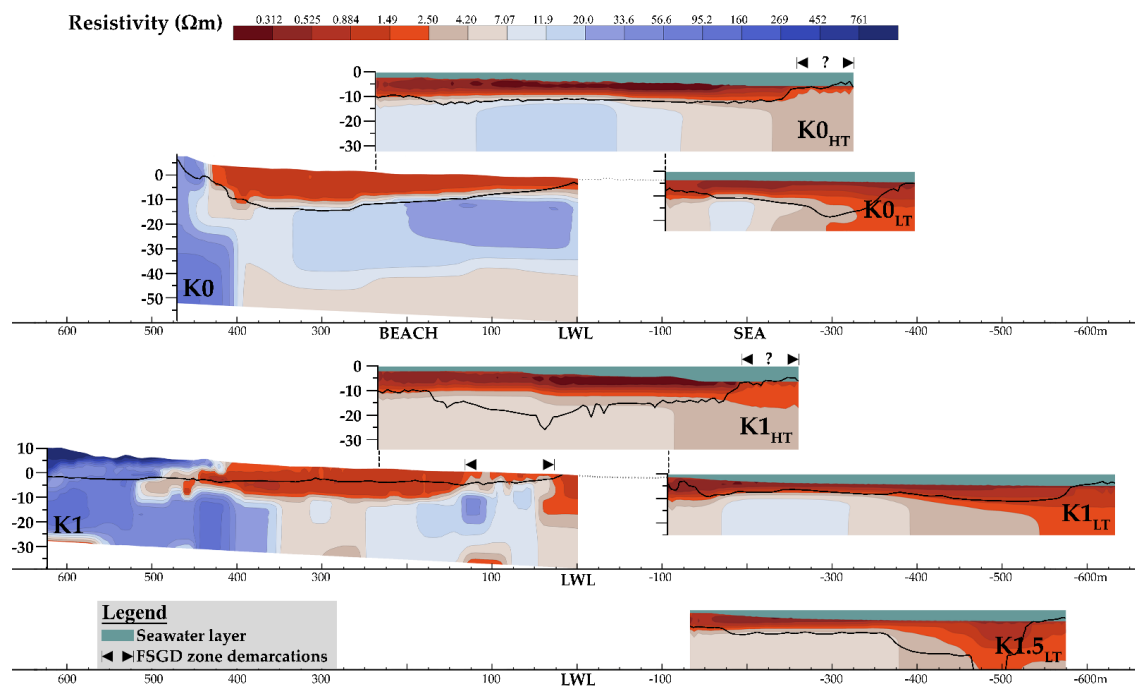
Figure 12. ERT profiles from De Westhoek (De Panne), modified from Paepen et al. [15]. LWL, HT, and LT stand for low water line, high tide, and low tide, respectively; note that the resistivity color scale is different since the formation factor is unlike that of Oostduinkerke; all profiles have the same scale length.
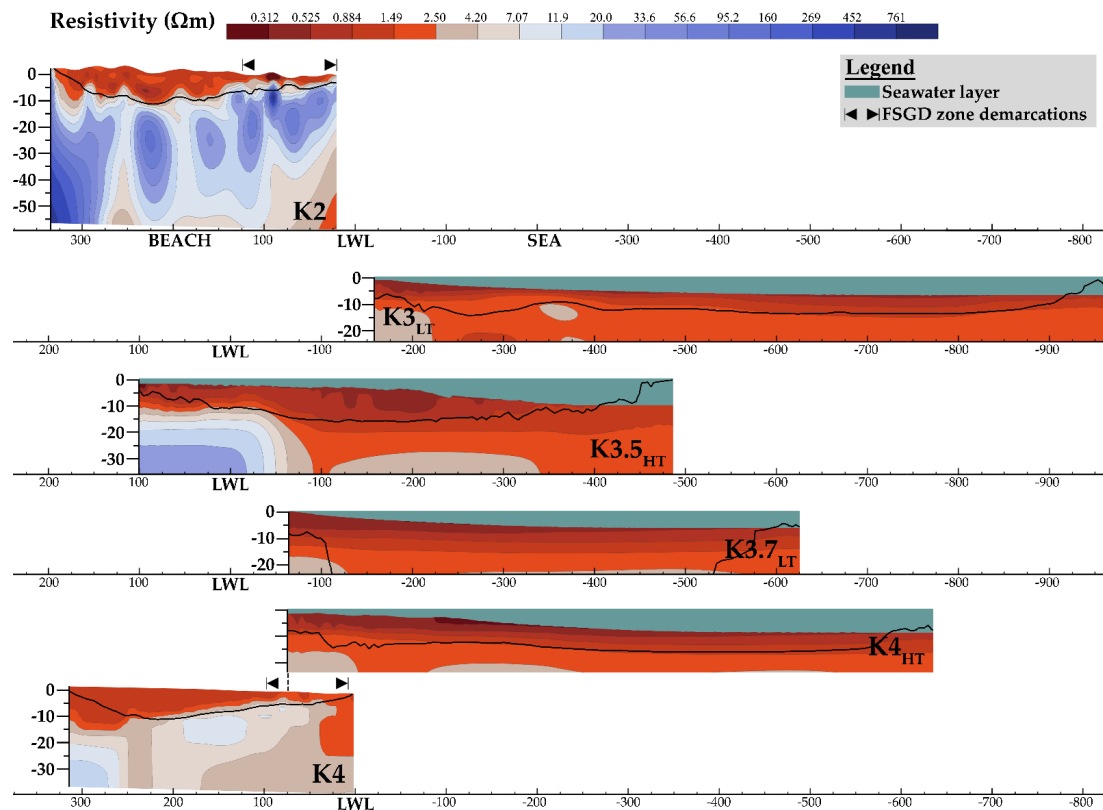

Figure 13. Land and marine ERT inversion models in front of De Westhoek nature reserve. LWL, HT, and LT stand for low water line, high tide, and low tide, respectively; note that the resistivity color scale is different since the formation factor is unlike that of Oostduinkerke; all profiles have the same scale length.

5. Discussion

5.1. Anthropogenic Effects on FSGD

For Sint-André, the zone in which the subterranean estuary contains pore water with a resistivity above 2.5 Ωm (brackish or fresh) extends furthest offshore in front of the largest MAR pond (K9.8), while it is the smallest in the east. The further this zone extends offshore, the stronger the groundwater flux is towards the North Sea [15], meaning that the flux is higher in front of the large Aquaduin infiltration pond (and K8.2) than in front of the municipality and the eastern part of the dunes. The infiltration causes a southward shift of the groundwater divide compared to a situation where only pumping would occur. The recharge zone of the FSGD is, therefore, expanded in size, allowing a larger volume to flow towards the North Sea.

The main influencing factors in this area are the hydraulic conductivity of the sediments (1), the hydraulic gradient between land and sea (2), groundwater infiltration (3) and extraction (4), the precipitation (5), and the rainwater infiltration capacity of the surface (6). The rainfall is similar in the entire zone and we can neglect run-off since the phreatic aquifer is sandy at the top, so the groundwater recharge is similar. The hydraulic conductivity is higher for coarser sediments; however, the heterogeneity of the aquifer is not well known for this area (especially offshore); only the site of Aquaduin has been thoroughly investigated. The situation in front of De Panne is different from Koksijde-Bad. FSGD is closer to or only on the beach (Figure 14). This is partly due to the De Westhoek extraction site that lies south of De Panne. However, the presence of a shallow clay lens at Koksijde-Bad allows for a larger hydraulic gradient between land and sea, yielding a stronger groundwater flux. However, the clay lens also pushes the water divide of the deeper aquifer closer to the sea [14] and decreases the infiltration capacity of the aquifer. Both affect the flux negatively. On the other hand, the MAR has increased the hydraulic heads even more in the municipality [8].
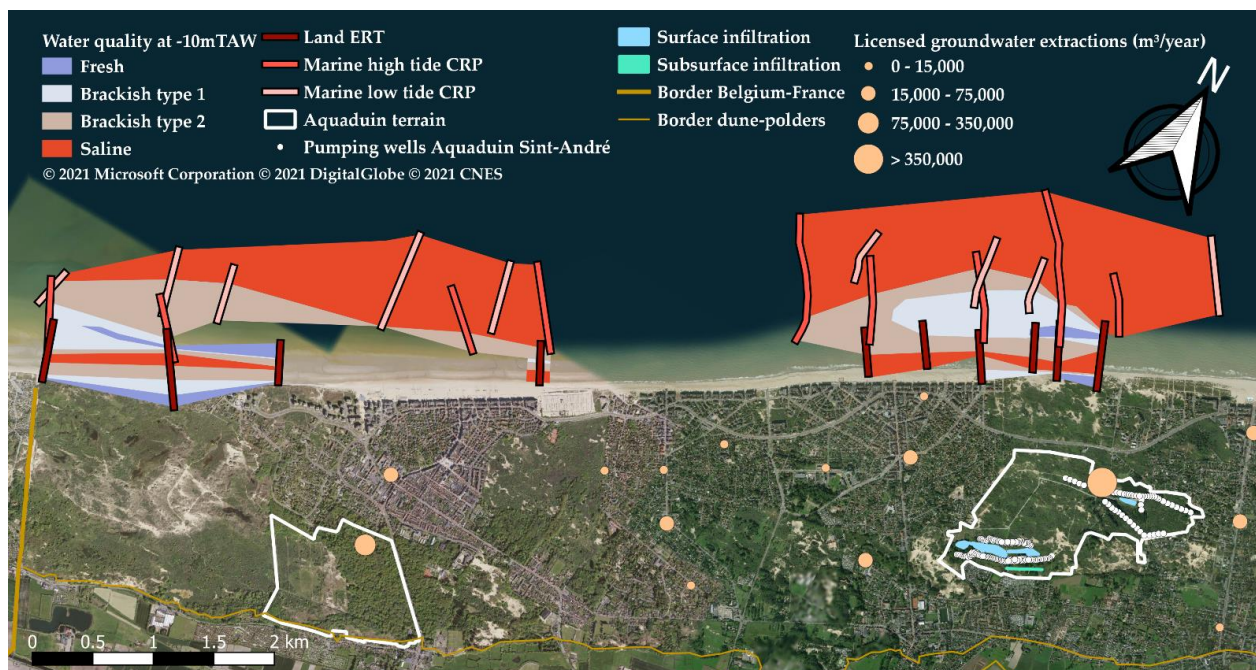
Figure 14. Map of the pore water quality of the most western part of the Belgian shoreline, based on inversion models of De Westhoek and Sint-André. Saline, brackish type 2 (between 2.5 and 4.2 Ωm for De Westhoek and 3.13 up to 8.84 Ωm at Sint-André), brackish type 1 (between 4.2 and 20 Ωm for De Westhoek and 8.84 up to 25 Ωm at Sint-André), and fresh pore water are distinguished. Note that the categories do not account for the estimation error resulting from inversion, meaning that brackish water could actually be fresh. Licensed extractions between 2018 and 2021 from DOV.

The extent of the brackish/freshwater lens in front of the largest MAR pond at Sint-André is similar to what we see at K0 and K1 in front of De Westhoek (Figure 14). Similar to observations at K0, there is no discharge on the lower beach. Therefore, the current pumping and infiltration rates result in FSGD, which is relatively similar to the natural state of the Western Belgian coastal zone.

5.2. Comparison with Existing Groundwater Models: De Westhoek

In 1969, water extraction started at De Westhoek. At the time, the water divide was positioned in the middle of the dunes [14]. A shallow clay layer allows for a water divide in the deeper aquifer to be positioned closer to the beach [14]. The extraction gradually increased from around 600,000 m^3/year up to a peak of 2 million m^3/year in 1989. This was leading to an increased chloride content in several wells due to the attraction of salty groundwater from the polders [14]. As a consequence of the increased pumping rate, the water divide was shifted northward (almost reaching the high water line in front of the extraction site at the maximum pumping rates), decreasing the FSGD recharge zone, which decreased the freshwater outflow and increased the thickness of the saltwater lens [14].

From 1994 onward, the pumping rates were decreased, especially for the well battery located closest to the polder [14]. Vandenbohede and Lebbe [30] made a groundwater model of the area, showing the situation in 2004. The pumping rate was just over 650,000 m^3 in that year [52], which is more than twice the current pumping rate. We can, therefore, assume that the freshwater outflow to the North Sea is stronger now (closer to the natural state) than it was back then in front of the extraction site.

The model was georeferenced in QGIS and compared to the geophysical data. It is clear that no outflow is expected above the low water line for the model layer of 1.95 mTAW (Figure 15). At K0, the Belgian–French border, the zone of freshwater discharge is seen just below the sea level. The offshore extent of the fresh to brackish discharge is similar for the field data and the groundwater model from the Belgian–French border up to just before K2. The outflow is more brackish in the field data (below 8.84 Ωm), which may be due to the inversion process that has led to lower resistivities of the freshwater lens.

The zone of discharge is around 200 m wide in the groundwater model and shifts northward towards the municipality of De Panne and the extraction facility (in the east). This is different from today's pattern, where a landward shift is observed from the resistivity data, in which a freshwater outflow is seen on the beach close to the extraction site and on the eastern end of De Panne. The field data show a smaller offshore extent of brackish/fresh porewater in front of the Aquaduin site and the municipality of De Panne compared to the hydrogeological model. The FSGD footprint may have changed due to the decrease in pumping rate, but, as noted above, this should lead to an increase in the discharge and a seaward shift of the discharge zone. Another explanation is that the groundwater model is not detailed enough, especially on the seaside, and might not include some heterogeneity of the aquifer (e.g., clay lenses) to simulate FSGD on the beach.

Figure 15. Comparison of the salinity around 1.95 mTAW modelled by Vandenbohede and Lebbe [30] with the porewater salinity at −10 mTAW based on the resistivity surveys. The fuchsia line provides an approximation of the low water line; the white lines on the groundwater model are the hydraulic head isolines, and the numbers are in mTAW; the color scale for the groundwater model is on the right-hand side; the legend for the inverted field data is on the bottom left.

5.3. Comparison with Existing Groundwater Models: Sint-André

Before the groundwater extraction started in 1949, the groundwater divide was situated more to the south, allowing more fresh groundwater to flow towards the sea [14,35]. From 1949 up to 2002, this groundwater flow decreased in magnitude and completely stopped due to the pumping of groundwater, allowing salt water to fill the entire phreatic aquifer under the beach [14]. In 2002, the artificial recharge was implemented to reduce the amount of natural groundwater that is pumped, which increased the freshwater heads again, although these are still lower than in the natural state, and the natural flow towards the North Sea was restored in most of the aquifer [14]. The freshwater tongue was also restored, underlying the saltwater lens [8].

The most recent groundwater model of the area was produced by Lebbe [8] in 2019. He investigated the situations in and after 2016 in the scope of a new permit of Aquaduin (for the extension of the surface pond, creation of a pond in the old rinse basin, construction of new pumping wells, and an increase in the extraction rate). We must take into account that the residence time of the water infiltrating around the water divide can be over 100 years [36]. The groundwater system needs some time to find a new equilibrium; therefore, the changes made in March 2019 (increased pumping and extension of the infiltration) might not be visible in the 2019, 2020, and 2021 surveys. The resistivities at −10 mTAW (Figure 14) from the ERT and CRP measurements are, therefore, compared with the situations in 2016 and 2030 from Lebbe's model [8] (Figure 15).

The groundwater model shows a lateral variation of FSGD and the saltwater lens (Figure 16). At K7.8 and K8.2 (Figures 10 and 11), the saltwater lens (resistivity below 3.13 Ωm) is seen on a small part of the upper beach at −10 mTAW, while it extends to the

lower beach in the two scenarios of the groundwater model (Figure 15). This might be due the slightly different depth interval of the model and the field data. Similarly, at K7.3, the saltwater lens comprises the full beach, while the field data indicates very brackish to brackish porewater (8.84 to 25 Ωm) (Figure 10).
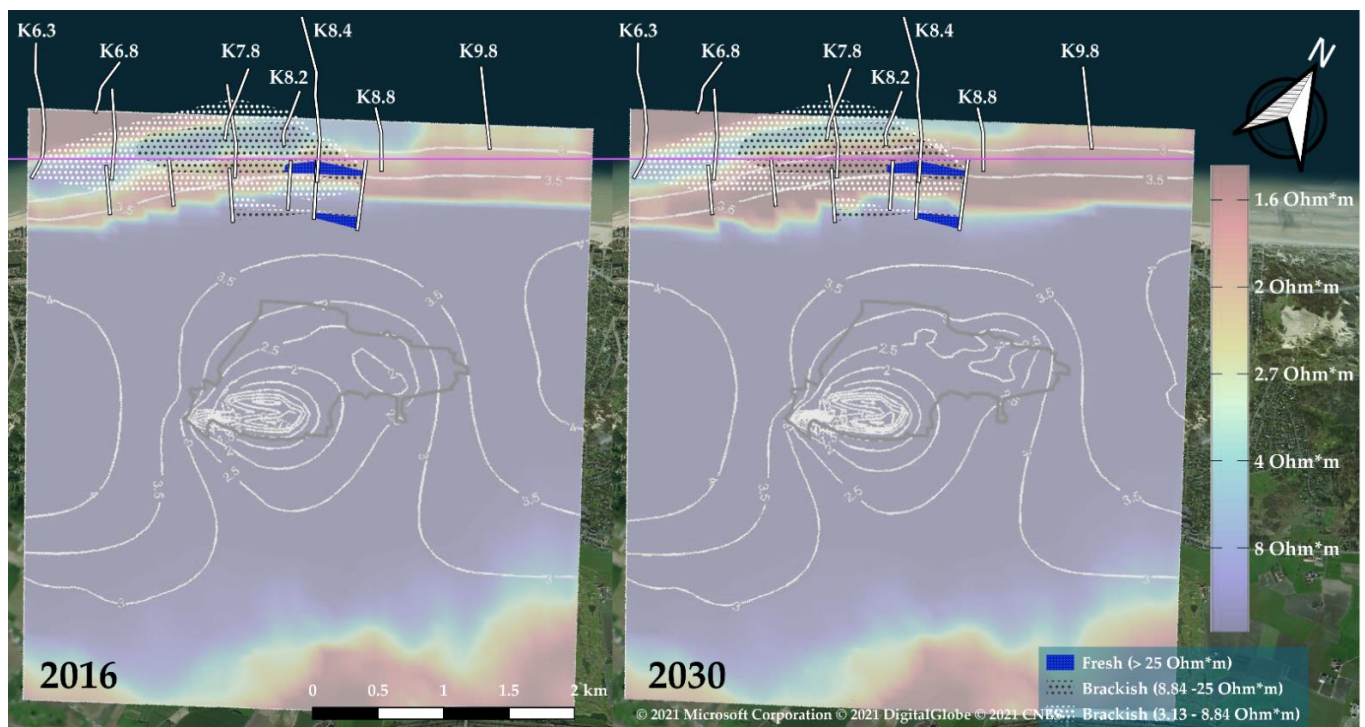
Figure 16. Comparison of the salinity between −9 and −9.5 mTAW modelled by Lebbe [8] with the porewater salinity at −10 mTAW based on the resistivity surveys; left: situation before the re-license, right: 11 years after the re-license of 2019. The fuchsia line provides an approximation of the low water line; the white lines on the groundwater models are the hydraulic head isolines, and the numbers are in mTAW; the color scale for the groundwater model is on the right-hand side; the legend for the inverted field data is on the bottom right.

The model scenarios even show that the saltwater lens extends further, below the low water line, in front of the Aquaduin site, while the field data indicate freshwater discharge on the lower beach in this zone (Figure 11, K8.4 to K8.8). This FSGD zone is not reproduced with the current groundwater model, and the model seems to overestimate the groundwater flux towards the sea further offshore. The phreatic aquifer in the model was built-up by four main units: sandy eolian dune deposits, more clayey polder deposits, alluvial cover layers, and Pleistocene deposits [8]. Heterogeneity within these units is not included, e.g., occurrence of more silty and clay layers [14], which might explain the differences mentioned here.

The saltwater lens becomes narrower towards Koksijde-Bad, getting completely cut-off by brackish to freshwater (above 4 Ωm) outflow on the lower beach in the west of the models. This is also displayed by the inversion models. They indicate very brackish porewater (below 8.84 Ωm) in this area (Figure 10, K6.3_{HT}, K6.8, and K6.8_{HT}). The inversion process, however, might have led to an underestimation of the resistivity in this zone. The outflow might be fresher than anticipated.

The depth of the saltwater lens will increase, according to Lebbe [8], in the coming years due to the re-licensing, in which more pumping will occur (up to over 25 m in 2040). At K8.4 and around K7.8, the groundwater models show a saltwater lens that is approximately 16 and 23 m thick in 2016 and 2030, respectively [8]. A lens of approximately 10 m thickness is seen in the inversion models, which is thinner than in both scenarios

of the hydrogeological model. The saltwater lens extent seems to be overestimated in the groundwater model in the lateral and vertical directions, which is likely due to the dimensions of the model cells (75 m $\times$ 75 m $\times$ 2.5 m).

The field data can be used to improve the groundwater model in the future. Local lithological heterogeneity must be included since it has an important impact on the FSGD footprint. The extent of local clay lenses is not well-known, especially offshore. New investigations are, therefore, needed. The groundwater model should also be extended more offshore since brackish porewater is seen beyond the northern boundary.

6. Conclusions

In this paper, we have investigated the ability of on-land electrical resistivity tomography (ERT) and marine continuous resistivity profiling (CRP) to identify fresh submarine groundwater discharge (FSGD) along the Belgian coast. Based on synthetic studies and the definition of thresholds on the normalized sensitivity and resolution matrix, we have identified which parts of the tomograms can be interpreted quantitatively, in terms of the salinization fraction, and qualitatively, in terms of the relative change in salinity. It appears that, generally, only the shallowest part of the inverted model can be interpreted quantitatively, in zones where the salinity is close to the seawater salinity or where freshwater is close to the surface. Errors on the estimated salinization fraction are maximal at the interfaces between fresh- and saltwater or at interfaces between different lithologies. Overall, the resistivity of FGSD is underestimated by the inversion process, simultaneously yielding an overestimation of the salinity. Although the quantitative interpretation of ERT and CRP is limited, both methods are able to identify lateral, and to a lesser extent vertical, changes in resistivity. They are, thus, particularly efficient in identifying the footprints of FSGD in coastal areas, although they have only limited added value for the quantification of the salinity.

We have applied the methodology to the ERT and CRP profiles collected in the western part of the Belgian coast, where zones both with and without human influences are found. We demonstrated that in natural conditions, the equilibrium between onshore aquifers and the sea leads FSGD to be situated below the low water line in this area. In case of significant water extraction, the FGSD moves towards the coast and can occur above the low water line in the intertidal zone or can even completely disappear. Artificial recharge compensating for water extraction can overcome this trend and can lead to a situation closer to natural conditions.

By comparing the identified FGSD zones with existing groundwater models, we were able to identify a discrepancy between the outcomes of the models and the actual situation. We hypothesize that this discrepancy can be related to a lack of data at sea, particularly the heterogeneous nature of the coastal aquifer that can be responsible for more complicated patterns of FGSD, as observed by the geophysical data. Given the importance of the FGSD component in the dynamics of coastal aquifers, we think that a more systematic acquisition of geophysical data, especially offshore, could fill the current gap in modelling efforts and should lead to the development of more robust groundwater models, helping in the management of coastal groundwater resources.

Author Contributions: M.P. conceptualized the survey plan, supervised the field work, applied the methodology, processed the data, prepared the original draft, created the figures, and acquired the funding for part of the field study. W.D. helped in conceptualizing the methodology, assisted in the field work, and reviewed and edited the manuscript. S.D.L. helped in the field investigation and contributed to the data processing. T.H. supervised, helped in conceptualizing the methodology, aided in the field work, and reviewed and edited the manuscript. K.W. supervised and reviewed and edited the manuscript. All authors have read and agreed to the published version of the manuscript.

References

1. Luijendijk, E.; Gleeson, T.; Moosdorf, N. Fresh groundwater discharge insignificant for the world's oceans but important for coastal ecosystems. *Nat. Commun.* **2020**, *11*, 1260. [CrossRef] [PubMed]
2. Bratton, J.E. The Three Scales of Submarine Groundwater Flow and Discharge across Passive Continental Margins. *J. Geol.* **2010**, *118*, 565–575. [CrossRef]
3. Moosdorf, N.; Oehler, T. Societal use of fresh submarine groundwater discharge: An overlooked water resource. *Earth Sci. Rev.* **2017**, *171*, 338–348. [CrossRef]
4. Santos, I.R.; Chen, X.; Lecher, A.L.; Sawyer, A.H.; Moosdorf, N.; Rodellas, V.; Tamborski, J.; Cho, H.-M.; Dimova, N.; Sugimoto, R.; et al. Submarine groundwater discharge impacts on coastal nutrient biogeochemistry. *Nat. Rev. Earth Environ.* **2021**, *2*, 307–323. [CrossRef]
5. Zamani, M.G.; Moridi, A.; Yazdi, J. Groundwater management in arid and semi-arid regions. *Arab. J. Geosci.* **2022**, *15*, 362. [CrossRef]
6. Braga, A.C.R.; Serrao-Neumann, S.; de Oliveira Galvão, C. Groundwater management in coastal areas through landscape scale planning: A systematic literature review. *Environ. Manag.* **2020**, *65*, 321–333. [CrossRef] [PubMed]
7. Masciopinto, C.; Vurro, M.; Palmisano, V.N.; Liso, I.S. A Suitable Tool for Sustainable Groundwater Management. *Water Resour. Manag.* **2017**, *31*, 4133–4147. [CrossRef]
8. Lebbe, L. *Grondwatermodel Van De Geplande Wijzigingen in Waterwinning Sint-André*; Universiteit Gent: Gent, Belgium, 2017; p. 140.
9. Werner, A.D.; Bakker, M.; Post, V.A.E.; Vandenbohede, A.; Lu, C.; Ataie-Ashtiani, B.; Simmons, C.T.; Barry, D.A. Seawater intrusion processes, investigation and management: Recent advances and future challenges. *Adv. Water Resour.* **2013**, *51*, 3–26. [CrossRef]
10. White, E.; Kaplan, D. Restore or retreat? Saltwater intrusion and water management in coastal wetlands. *Ecosyst. Health Sustain.* **2017**, *3*, e01258. [CrossRef]
11. Van Houtte, E.; Verbauwhede, J. Environmental benefits from water reuse combined with managed aquifer recharge in the Flemish dunes (Belgium). *Int. J. Water Resour. Dev.* **2021**, *37*, 1027–1034. [CrossRef]
12. Bachtouli, S.; Comte, J.-C. Regional-scale analysis of the effect of managed aquifer recharge on saltwater intrusion in irrigated coastal aquifers: Long-term groundwater observations and model simulations in NE Tunisia. *J. Coast. Res.* **2019**, *35*, 91–109. [CrossRef]
13. Dillon, P. Future management aquifer recharge. *Hydrogeol. J.* **2005**, *13*, 313–316. [CrossRef]
14. Vandenbohede, A.; Van Houtte, E.; Lebbe, L. Sustainable groundwater extraction in coastal areas: A Belgian example. *Environ. Geol.* **2008**, *57*, 735–747. [CrossRef]
15. Paepen, M.; Hanssens, D.; De Smedt, P.; Walraevens, K.; Hermans, T. Combining resistivity and frequency domain electromagnetic methods to investigate submarine groundwater discharge (SGD) in the littoral zone. *Hydrol. Earth Syst. Sci.* **2020**, *24*, 3539–3555. [CrossRef]
16. Cantarero, D.L.M.; Blanco, A.; Cardenas, M.B.; Nadaoka, K.; Siringan, F.P. Offshore Submarine Groundwater Discharge at a Coral Reef Front Controlled by Faults. *Geochem. Geophys. Geosystems.* **2019**, *20*, 8310. [CrossRef]
17. Goebel, M.; Pidlisecky, A.; Knight, R. Resistivity imaging reveals complex pattern of saltwater intrusion along Monterey coast. *J. Hydrol.* **2017**, *551*, 746–755. [CrossRef]
18. Cong-Thi, D.; Pham Dieu, L.; Thibaut, R.; Paepen, M.; Hieu Ho, H.; Nguyen, F.; Hermans, T. Imaging the Structure and the Saltwater Intrusion Extent of the Luy River Coastal Aquifer (Binh Thuan, Vietnam) Using Electrical Resistivity Tomography. *Water* **2021**, *13*, 1743. [CrossRef]
19. González-Quirós, A.; Comte, J.-C. Relative importance of conceptual and computational errors when delineating saltwater intrusion from resistivity inverse models in heterogeneous coastal aquifers. *Adv. Water Resour.* **2020**, *144*, 103695. [CrossRef]
20. Day-Lewis, F.D.; Singha, K.; Binley, A.M. Applying petrophysical models to radar travel time and electrical resistivity tomograms: Resolution-dependent limitations. *J. Geophys. Res.* **2005**, *110*, 3569. [CrossRef]
21. Binley, A.; Kemna, A. DC Resistivity and Induced Polarization Methods. In *Hydrogeophyscis*; Rubin, Y., Hubbard, S.S., Eds.; Springer: Dordrecht, The Netherlands, 2005; Volume 50.

22. Caterina, D.; Beaujean, J.; Tanguy, R.; Nguyen, F. A comparison study of different image appraisal tools for electrical resistivity tomography. *Near Surf. Geophys.* **2013**, *11*, 639–657. [CrossRef]

23. Wilson, S.R.; Ingham, M.; McConchie, J.A. The applicability of earth resistivity methods for saline interface definition. *J. Hydrol.* **2006**, *316*, 301–312. [CrossRef]

24. Comte, J.-C.; Banton, O. Cross-validation of geo-electrical and hydrogeological models to evaluate seawater intrusion in coastal aquifers. *Geophys. Res. Lett.* **2007**, *34*, L10402. [CrossRef]

25. Nguyen, F.; Kemna, A.; Antonsson, A.; Engesgaard, P.; Kuras, O.; Ogilvy, R.; Gisbert, J.; Jorreto, S.; Pulido-Bosch, A. Characterization of seawater intrusion using 2D electrical imaging. *Near Surf. Geophys.* **2009**, *7*, 377–390. [CrossRef]

26. Beaujean, J.; Nguyen, F.; Kemna, A.; Engensgaard, P. Joint and sequential inversion of geophysical and hydrogeological data to characterize seawater intrusion models. In Proceedings of the 21st Salt Water Intrusion Meeting, Ponta Delgada, Portugal, 21–25 June 2010; pp. 57–60.

27. Hermans, T.; Vandenbohede, A.; Lebbe, L.; Martin, R.; Kemna, A.; Beaujean, J.; Nguyen, F. Imaging artificial salt water infiltration using electrical resistivity tomography constrained by geostatistical data. *J. Hydrol.* **2012**, *438–439*, 168–180. [CrossRef]

28. Zeynolabedin, A.; Ghiassi, R.; Norooz, R.; Najib, S.; Fadili, A. Evaluation of geoelectrical models efficiency for coastal seawater intrusion by applying uncertainty analysis. *J. Hydol.* **2021**, *603*, 127086. [CrossRef]

29. Taniguchi, M.; Dulai, H.; Burnett, K.M.; Santos, I.R.; Sugimoto, R.; Stieglitz, T.; Kim, G.; Moosdorf, N.; Burnett, W.C. Submarine Groundwater Discharge: Updates on Its Measurement Techniques, Geophysical Drivers, Magnitudes, and Effects. *Front. Environ. Sci.* **2019**, *7*, 141. [CrossRef]

30. Vandenbohede, A.; Lebbe, L. *De Panne—Natuurreservaat—De Westhoek Monitoring Grondwater Slufters. Fase 2*; Universiteit Gent: Gent, Belgium, 2008.

31. Baeteman, C. The Holocene depositional history of the IJzer palaeovalley (Western Belgian coastal plain) with reference to the factors controlling the formation of intercalated peat beds. *Geol. Belg.* **1999**, *2*, 39–72. [CrossRef]

32. Van Meir, N.; Lebbe, L. Simulations of Evolution of Salt-Water Distribution in Young Dunes near the French-Belgian Border. *Nat. Tijdschr.* **1997**, *79*, 105–113.

33. Baeteman, C. Chronology of coastal plain development during the Holocene in West Belgium. *Quaternaire* **1991**, *2*, 116–125. [CrossRef]

34. De Breuck, W.; De Moor, G.; Maréchal, R.; Tavernier, R. Diepte van het grensvlak tussen zoet en zout water in de freatisch laag van het Belgische kustgebied (1963–1973). In *Verziltingskaart*; Militair Geografisch Instituut: Brussel, Belgium, 1974.

35. Vandenbohede, A.; Van Houtte, E.; Lebbe, L. Water quality changes in the dunes of the western Belgian coastal plain due to artificial recharge of tertiary treated wastewater. *Appl. Geochem.* **2009**, *24*, 370–382. [CrossRef]

36. Vandenbohede, A.; Lebbe, L. Occurrence of salt water above fresh water in dynamic equilibrium in a coastal groundwater flow system near De Panne, Belgium. *Hydrogeol. J.* **2006**, *14*, 462–472. [CrossRef]

37. Vandenbohede, A.; Van Houtte, E.; Lebbe, L. Groundwater flow in the vicinity of two artificial recharge ponds in the Belgian coastal dunes. *Hydrogeol. J.* **2008**, *16*, 1669–1681. [CrossRef]

38. Lebbe, L.; De Breuck, W. Hydrogeologie van het duingebied tussen Koksijde en Oostduinkerke. *Tijdschr. Van Het Belg. Cent. Voor De Stud. Van Water Bodem En Lucht* **1980**, *55*, 33–45.

39. Lebbe, L. Hydrogeologie van het duingebied ten westen van De Panne. In *Docoraatsverhandeling*; Rijksuniversiteit Gent: Gent, Belgium, 1978.

40. Lebbe, L. Litostratigrafie en hydraulische doorlatendheid van het freatische reservoir te De Panne. *Nat. Tijdschr.* **1979**, *61*, 29–58.

41. Van Houtte, E.; Verbauwhede, J. Switching Between Open And Subsurface Infiltration According To Temperature. In Proceedings of the 48th IAH Congress, Brussels, Belgium, 6–10 September 2021; pp. 103–104.

42. IWVA. *Jaarverslag 2019*; IWVA: Koksijde, Belgium, 2019; p. 58.

43. Martens, K.; Walraevens, K.; Lebbe, L. *Ecosysteemvisie Voor De Vlaamse Kust—Deelstudie: Hydrogeologie Synthese*; Universiteit Gent—Toegepaste Geologie en Hydrogeologie: Gent, Belgium, 1995.

44. Lebbe, L. Parameter identifcation in fresh-saltwater flow based on borehole resistivities and freshwater head data. *Adv. Water Resour.* **1999**, *22*, 791–806. [CrossRef]

45. Vandenbohede, A.; Lebbe, L.; Gysens, S.; Delecluyse, K.; Dewolf, P. Salt water infiltration in two artificial sea inlets in the Belgian dune area. *J. Hydrol.* **2008**, *360*, 77–86. [CrossRef]

46. Dahlin, T.; Zhou, B. Multiple-gradient array measurements for multichannel 2D resistivity imaging. *Near Surf. Geophys.* **2006**, *4*, 113–123. [CrossRef]

47. Loke, M.H. *Rapid 2-D Resistivity & IP Inversion Using the Least-Squares Method*; Geotomo Software: Penang, Malaysia, 2011; p. 152.

48. De Breuck, W.; De Moor, G. The water-table aquifer in the Eastern coastal area of Belgium. *Hydrol. Sci. J.* **1969**, *14*, 137–155. [CrossRef]

49. Oldenburg, D.W.; Li, Y. Estimating depth of investigation in dc resistivity and IP surveys. *Geophysics* **1999**, *64*, 403–416. [CrossRef]

50. Kemna, A. *Tomographic Inversion of Complex Resistivity: Theory and Application*; Ruhr-Universität Bochum: Osnabrück, Germany, 2000.

51. Lebbe, L. The subterranean flow of fresh and salt water underneath the Western Belgian beach. In Proceedings of the 7th Salt Water Intrusion Meeting, Uppsala, Sweden, 14–17 September 1981; pp. 193–219.

52. IWVA. *Jaarrapport 2005*; IWVA: Koksijde, Belgium, 2005; p. 47.